Applications of Fiber-top Technology for Material Property Characterization at Nanoscale

Chavan, D.C.

2014

document version
Publisher's PDF, also known as Version of record

Applications of *Fiber-top* Technology for Material Property Characterization at Nanoscale

Dhwajal Chandrakant Chavan

Applications of *Fiber-top* Technology for Material Property Characterization at Nanoscale

Dhwajal Chandrakant Chavan

Printed by Ipskamp Drukkers
Cover design: Center picture of the cover designed by prof. dr. Davide Iannuzzi & was selected as cover page for Journal of Microscopy, April 2011 issue.

VRIJE UNIVERSITEIT

Applications of *Fiber-top* Technology for Material Property Characterization at Nanoscale

ACADEMISCH PROEFSCHRIFT

ter verkrijging van de graad Doctor aan
de Vrije Universiteit Amsterdam,
op gezag van de rector magnificus
prof.dr. F.A. van der Duyn Schouten,
in het openbaar te verdedigen
ten overstaan van de promotiecommissie
van de Faculteit der Exacte Wetenschappen
op maandaag 13 januari 2014 om 11.45 uur
in de aula van de universiteit,
De Boelelaan 1105

door

Dhwajal Chandrakant Chavan
geboren te Baroda, India

promotor: prof.dr. D. Iannuzzi

Reading committee:

prof.dr. J. Dankelman, Delft University of Technology, The Netherlands
dr. N. Tas, University of Twente, The Netherlands
prof.dr. T. H. Smit, Vrije Universiteit Medical Centre Amsterdam, The Netherlands
dr. W. H. Roos, Vrije Universiteit Amsterdam, The Netherlands

This work was funded by the European Research Council (ERC), the Netherlands Organization for Scientific Research (NWO) and the Stichting voor Fundamenteel Onderzoek der Materie (FOM).

Contents

Chapter -1

Introduction

The chapter introduces briefly the field of material science research and scanning probe microscopy. It discusses some of its limitations and presents the concept of fiber-top technology as an alternative to conventional scanning probe microscopy systems. This chapter also outlines the scope and objective of the research activity and how this thesis is organized.

1.1 SURFACE CHARACTERIZATION AT NANOSCALE

Material science is one of the oldest disciplines of science, wherein physical, chemical, thermal, atomic, electrical and optical properties of a material are investigated. Conventional material science studies on bulk metals and ceramics has matured over the time, and, now encompasses various classes of materials like polymers, biomaterials, thin films and semiconductors. Numerous methods are used routinely for material analysis and characterization. Each of these analysis methods has its specific application area for certain class of materials, and certain limitations based on testing conditions, operating principle, measurement resolution, sample size and sample physical state. One such method that has developed and matured significantly over the last three decades is scanning probe microscopy (SPM).

Since the invention of the scanning tunneling microscope (STM) [1] and the atomic force microscope (AFM) [2], both categorized as SPM techniques, many variations based on the principle of SPM have developed. These extended SPM techniques like (near field optical microscopy (SNOM) [3], various scanning force microscopy (SFM) [4-6], scanning thermal microscopy (SThM) [7] and scanning electrochemical microscopy (SEcM) [8]) were developed for specific applications of scientific interests. AFMs are also used widely to study the mechanical properties of samples and the technique is referred as Nanoindentation. Owing to high sensitive force measurement capability of the AFMs (piconewton), they are also used to study fundamental forces like the Casimir force [9]. Use of AFMs is also demonstrated for novel applications like nanolithography [10, 11] and data storage [12].

These developments made significant contribution to the field of surface science, as it enabled to investigate nanoscale surface properties for the first time. The basic working principle of SPM is shown in Fig. 1.1, wherein an

ultra sharp tip at the end of a cantilever scans over the surface in a raster pattern to produce very high resolution 3D image of the sample surface. While the tip is being scanned, the optical triangulation records the deflection of the cantilever and the close-loop extends or retracts the piezoelectric stage to maintain a constant tip force. This mode of operation, known as *contact mode* imaging, can provide topography of the sample surface with sub-nanometer resolution.

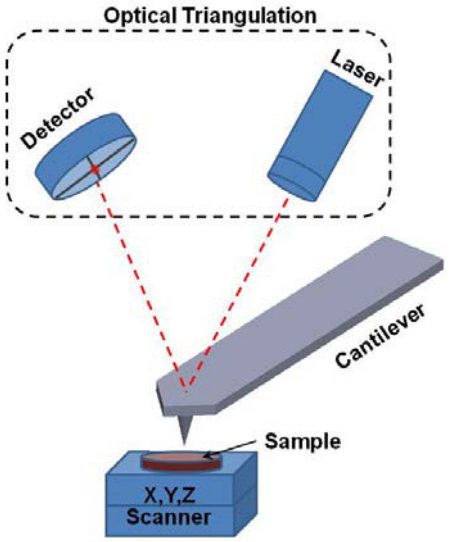

Fig. 1.1 Working principle of scanning probe microscopy.

In other imaging techniques like *non-contact mode* imaging [13, 14], the cantilever tip is not brought in contact with the sample but made to vibrate very close to the sample surface making intermittent (-quasi) contacts while scanning over the sample. This mode results in a lesser force exerted on the sample and hence lesser sample deformation.

In recent years, developments in field of electronics hardware, computational power and precision mechanics has improved the performance of AFMs by many folds and has made it an indispensible scientific tool. In spite of this overwhelming success, challenges still remain to make AFM a user friendly tool for industrial applications and improve existing techniques in terms of additional functionality, resolution and speed. AFM use in industrial environment has been limited, primarily due to complexity of the instrument and prerequisite of a trained professional to operate the instrument. Hence, further development of making the AFM handling more users friendly will extend its sphere of application.

In this thesis, a novel concept, called *fiber-top* and *ferrule-top* probes, is introduced along with series of experiments how these probes presents a unique opportunity to overcome some of the challenges faced by the conventional AFM systems.

1.2 A NOVEL APPROACH: FIBER-TOP TECHNOLOGY

In 2006 a novel approach was proposed to fabricate a cantilever at the end of an optical fiber. For proof-of-concept, a cantilever was carved at the end face of an optical fiber using a focused ion beam (FIB) milling technique [15]. A scanning electron microscope image of a *fiber-top cantilever* is shown in Fig. 1.2 (a); Fig. 1.2 (b) shows the readout schematic used to detect the deflection of the cantilever. When a laser is shone from the other end of the optical fiber, it travels along the optic fiber core and emerges at the face of the optical fiber. Part of this light reflects back and a part transmits further to be reflected by the surfaces of the cantilever. These reflected signals travel back through the same optical fiber and are redirected on a photodiode. The output of the photodiode is a sinusoidal function of the separation gap between the cantilever surface and the cleaved surface of the optical fiber [16]. With this detection scheme, the fiber-top cantilever deflection can be

measured by the interferometer with sub-nanometer resolution. This makes fiber-top cantilevers fully optical, monolithic and ultra compact sensors. Application of fiber-top cantilever was successfully demonstrated for sensing hydrogen [17] and measuring refractive index of liquids [18].

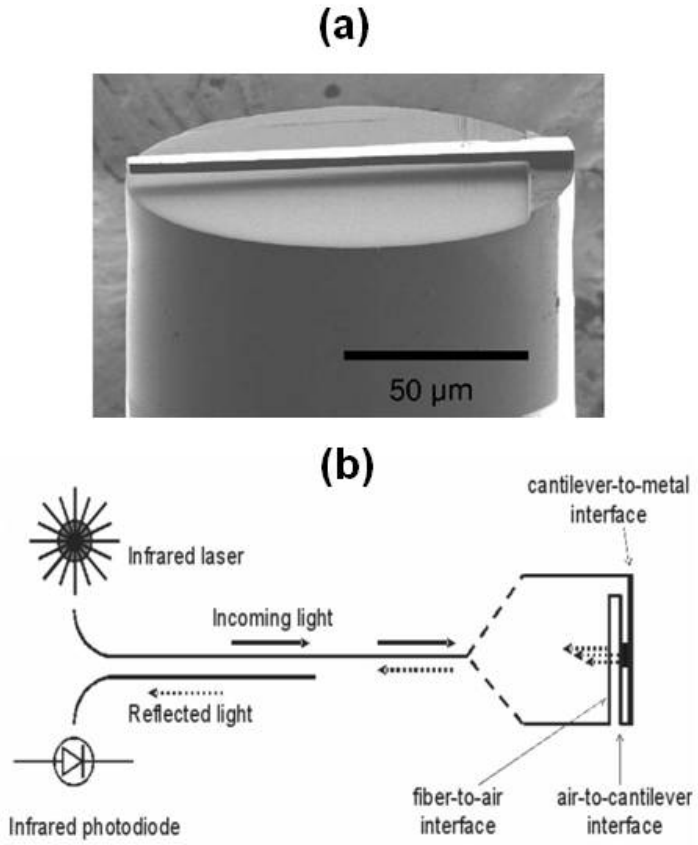

Fig. 1.2 (a) Scanning electron microscopy (SEM) image of micro cantilever fabricated on top of an optical fiber; (b) Detection scheme for fiber-top cantilever.

Fiber-top cantilevers with their self-aligned design (cantilever carved exactly on top of the core of an optical fiber), hold a unique advantage when compared to a conventional AFM alignment procedure. For fiber-top probes used for AFM application, a pyramidal tip is carved at the end of the cantilever. Such a fiber-top cantilever probe was used to demonstrate the first contact mode fiber-top AFM [19].

Fiber-top cantilever probes, are a promising approach for sensing and atomic force microscopy. However, this technology faces the challenge of cost effective fabrication. Presently, fiber-top cantilever probes are fabricated using focused ion beam (FIB) milling, which makes them extremely expensive. To address this issue, a novel cost effective concept of using ferruled optical fiber was introduced [20].

In this new concept, called *ferrule-top technology*, a cantilever is fabricated on top of a glass ferrule using a cost effective laser ablation micromachining process. This makes the fabrication of fiber-top like probes more cost effective while maintaining all the advantages of fiber-top cantilever probes.

1.3 SCOPE AND OBJECTIVES OF THIS THESIS

As seen in previous sections, application areas of scanning probe microscopy and material property characterization has extended enormously in recent times. This has presented unique opportunity for innovative concepts like fiber-top technology to demonstrate its potential.

The work presented in this thesis aims at developing the fiber-top technology in order to make it accessible to larger scientific community. With series of experiments demonstrated in this thesis work, we present fiber-top technology as an alternative to existing scanning probe microscopy with newer functional capabilities. To perform these experiments significant effort was made on development of the sensor readout system, experimental setup mechanics, control system and software modules. The thesis is further divided in six chapters with each chapter focusing on the specific application area of fiber-top and ferrule-top technology.

Chapter 2 highlights some of the fabrication challenges for fiber-top probes and presents an alternative cost effective fabrication process called *ferrule-top technology.* The chapter describes in detail the fabrication process for the new probe, the measurement setup, control system and successfully demonstrates the first ferrule-top atomic force microscope capable of contact mode imaging in air and liquids.

In **Chapter 3**, we aim at extending the capability of ferrule-top technology for imaging at low temperature (12 K), non-contact mode imaging, adaptability to commercial AFM systems and high speed imaging. These capabilities are demonstrated in two different experiments. In one experiment the ferrule-top probe is mounted on a commercial low temperature AFM for imaging in contact and non-contact mode at 12 K. In another experiment, we successfully integrate the ferrule-top probe onto a high speed AFM system and demonstrate imaging at rate of 2 frames per second.

Chapter 4 describes one of the most important capabilities of fiber-top/ferrule-top technology, namely the ability of coupling light to/from the sample, at nanoscale. Here, in two different experiments we demonstrate combined optical and scanning probe microscopy capability of fiber-top and ferrule-top probes.

Chapter 5 focuses on an important application area of nanoindentation for material property characterization using ferrule-top cantilever probes. The chapter describes the modified fabrication process for nanoindentation probe, the experimental setup, data analysis and results of nanoindentation tests on polymer sample in air and liquid.

Chapter 6 describes a novel fabrication approach that allows combining optical coherence tomography (OCT) with ferrule-top nanoindentation. This new probe can perform nanoindentation and simultaneously measures the deformation of layers within the sample at the point of indentation.

Chapter 7 presents a prototype of a nanoindenter based on ferrule-top technology with commercial mindset, i.e. designed for specific user application and specification with cost effective approach. The aim is to demonstrate application of ferrule-top nanoindentation for pre-clinical material property research. Addition to this future application areas of ferrule-top technology are discussed followed by thesis conclusion.

Considerable part of experiments and applications described in this thesis were performed in collaboration with other research groups and industry partners. The work presented in this thesis was funded by the European Research Council (ERC), the Netherlands Organisation for Scientific Research (NWO), the Stichting voor Fundamenteel Onderzoek der Materie (FOM).

REFERENCES

[1] G. Binnig, H. Rohrer, C. Gerber, and E. Weibel, Phys. Rev. Lett. 49, 57(1982).

[2] G. Binnig, C. F. Quate, and Ch. Gerber, Phys. Rev. Lett. 56, 930 (1986).

[3] D. W. Pohl, W. Denk, and M. Lanz, Appl. Phys. Lett. 44, 651(1984).

[4] Y. Martin, C. C. Williams, and H. K. Wickramasinghe, J. Appl. Phys. 61, 4723 (1987).

[5] V. Scherer, B. Bhushan, U. Rabe, and W. Arnold, IEEE Trans. Magn. 33, 4077 (1997).

[6] Y. Martin, and H. K. Wickramasinghe, Appl. Phys. Lett. 50, 1455 (1987).

[7] C. C. Williams, and H. K. Wickramasinghe, Appl. Phys. Lett. 49, 1587 (1986).

[8] O. E. Husser, D. H. Craston, and A. J. Bard, J. Electrochem. Soc. 136, 3222 (1989).

[9] S. de Man, K. Heeck, R. J. Wijngaarden, and D. Iannuzzi, Phys. Rev. Lett. 103, 040402 (2009).

[10] R. D. Piner, J. Zhu, F. Xu, S. Hong, and C. A. Mirkin, *Science* 283, 661 (1999).

[11] S. Deladi, N. R. Tas, J. W. Berenschot, G. J. M. Krijnen, M. J. de Boer, J. H. Boer, M. Peter, and M. C. Elwenspoek, Appl. Phys. Lett. 85, 5361 (2004).

[12] P. Vettiger, M. Despont, U. Drechsler, U. Dürig, W. Häberle, M.I. Lutwyche, H.E. Rothuizen, R. Stutz, R. Widmer, and G.K. Binnig, J. Res. Dev. 44, 323 (2000).

[13] Y. Martin, C. C. Williams, and H. K. Wickramasinghe, J. Appl. Phys. 61, 4723 (1987).

[14] D. Sarid, and V. Elings, J. Vac. Sci. Technol. B 9, 431 (1991).

[15] D. Iannuzzi, S. Deladi, V. J. Gadgil, G. P. Sanders, H. Schreuders, & M. C. Elwenspoek, Appl. Phys. Lett. 88, 053501 (2006).

[16] D. Rugar, H. J. Mamin, and P. Guethner, Appl. Phys. Lett. 55, 2588 (1989).

[17] D. Iannuzzi, S. Deladi, M. Slaman, J. H. Rector, H. Schreuders, and M. C. Elwenspoek, Sensors and Act. B 121, 706 (2007).

[18] C. J. Alberts, S. de Man, J. W. Berenschot, V. J. Gadgil, M.C. Elwenspoek, and D. Iannuzzi, Meas. Sci. Techn. 20, 034005 (2009).

[19] D. Iannuzzi, S. Deladi, J. W. Berenschot, S. de Man, K. Heeck, and M. C. Elwenspoek, Rev. Sci. Instrum. 77, 106105 (2006).

[20] G. Gruca, S. de Man, M. Slaman, J. H. Rector, and D. Iannuzzi, Meas. Sci. Technol. 2, 094033 (2010).

Chapter -2

Scanning Probe Microscopy - I

Ferrule-top cantilevers are a new generation of all-optical miniaturized devices for utilization in liquids, harsh environments, and small volumes. They are obtained by carving the end of a ferruled fiber in the form of a mechanical beam. Light coupled from the opposite side of the fiber allows detection of cantilever deflections. In this chapter, we demonstrate that ferrule-top cantilevers can be used to develop ultra compact AFMs for contact mode imaging in air and in liquids with sensitivity comparable to that of commercial AFMs.

Adapted from: "Ferrule-top atomic force microscope"
REVIEW OF SCIENTIFIC INSTRUMENTS 81, 123702 (2010).
D. Chavan, G. Gruca, S. de Man, M. Slaman, J. H. Rector, K. Heeck, and D. Iannuzzi

2.1 INTRODUCTION

Since its invention in 1986 [1] atomic force microscopy has witnessed an ever increasing popularity. Today, the atomic force microscope (AFM) is considered a unique instrument for its ability to provide surface topology images, force measurements, and information on material properties at the nanoscale. It is thus not surprising to notice that many research groups belonging to both the academic and the industrial environment have been continuously proposing new solutions to improve the performance of their AFMs, from novel imaging modes [2, 3] to high speed [4–6] and video rate scanning [7]. In spite of this impressive progress, in most commercially available AFMs the deflection of the cantilever is still detected by means of optical triangulation. However optical triangulation requires a volume of several cm^3, making further miniaturization virtually impossible. Furthermore, it does not adapt well to applications beyond research laboratories, where untrained personnel might not be comfortable with the alignment procedure necessary to bring the laser spot on the cantilever before utilization. Alternative detection schemes, like, for example, piezoresistive sensing [8], can be hardly used in liquid environments. There is thus an evident need of a compact, all-optical probe that overcomes the alignment procedure.

In 2006, our group has proposed a new generation of miniaturized devices that may solve this issue: the fiber-top cantilever [9, 10]. In a fiber-top probe, the cantilever is carved at the center of the cleaved end of an optical fiber. Light coupled from the opposite side of the fiber can then be used to detect the deflection of the cantilever. The probe is extremely compact (it is machined on a 125 μm diameter fiber), all optical, and very easy to use (the operator only needs to plug the fiber to the readout system). Unfortunately, fiber-top cantilevers are currently produced by means of a very expensive process (namely, Focused Ion Beam milling [11]). To solve this problem, at the beginning of 2010 we introduced a new approach to fiber-top probes, which now goes under the name of *ferrule-top cantilevers* [12, 13]. Ferrule top cantilevers are obtained by carving a cantilever out of a ferruled optical

fiber. Because the dimensions of a ferrule are more than one order of magnitude larger than those of a fiber, the fabrication process can rely on steps that adapt better to cost effective series production. In this chapter, we show that it is possible to equip a ferrule-top cantilever with a sharp conical tip for AFM purposes. The ferrule-top probe is then mounted on an extremely compact AFM, where it is used for contact mode imaging in both air and water.

2.2 FABRICATION AND READOUT

Ferrule-top cantilever probes, the macro version of fiber-top cantilevers are obtained via the fabrication steps illustrated in Fig. 2.1. The building block is a 2.5 mm × 2.5 mm × 7 mm pierced ferrule made out of borosilicate glass (VitroCom Inc.), with a central bore hole that has a diameter of 127 μm [Fig. 2.1(i)]. The ferrule is initially mounted on the stage of a ps-laser ablation machine (Optec System with Lumera Laser source), where, following the steps described in Refs. 12 and 13, it is machined into a 220 μm wide, 200 μm thick rectangular ridge [Fig. 2.1(ii)]. The ablation machine is then used to carve a 50 μm × 50 μm suspended square hole at the end of the ridge and a v-groove on the side of the ferrule [Figs. 2.1(iii) and 2.2]. After the ferrule is taken out of the ablation machine, a GeO2 doped single mode silica fiber (Fibercore Ltd.), equipped with an ~8 μm high, ~100 nm radius conical tip [14], is laid on the v-groove, slid into the rectangular hole, and glued to the ridge [Figs. 2.1(iv) and 2.2]. The ferrule is then mounted again on the stage of the ps-laser ablation machine to carve the ridge in the form of a tipped cantilever [Figs. 2.1(v) and 2.3]. The length and the width of the cantilever can be controlled within the cutting resolution of the laser ablation system (approximately 5 μm).

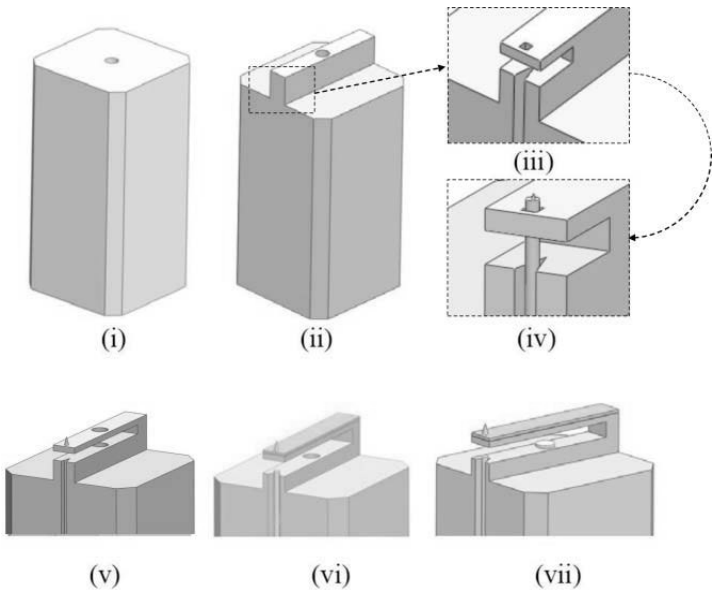

Fig. 2.1 Illustration of the fabrication steps followed for the production of tipped ferrule-top cantilevers (not to scale): (i) the building block is a 2.5 mm × 2.5 mm × 7 mm pierced ferrule made out of borosilicate glass (diameter of the central bore = 127 μm); (ii) the top of the ferrule is machined in a form of a 220 μm wide, 200 μm thick rectangular ridge; (iii) one side of the ridge is machined to host an ≈50 μm diameter fiber; (iv) a ≈50 μm diameter fiber with a conical sharp tip on its end is glued to the ridge; (v) the ridge is further machined in a form of a cantilever (undercut); (vi) a droplet of glue is placed inside the hole at the center of the cantilever, and the probe is coated with a thin gold layer; (vii) a standard single mode optical fiber is inserted into the bore of the ferrule and glued.

The thickness of the cantilever is more difficult to control, and is limited to 10 μm reproducibility. Because of those limitations, we generally carve

cantilevers that are 2200–2300 μm long, 215–225 μm wide, and 20–30 μm thick, which correspond to spring constants between 8 and 20 N/m and resonance frequencies between 5 and 7 kHz. At the end of the carving process, the residual hole at the center of the cantilever is filled with ultraviolet (UV) curable glue. The probe is then put inside a sputtering system, where it is coated with a 5 nm thick Cr layer followed by a 30 nm thick Au film [Fig. 2.1(vi)]. Finally, a single mode optical fiber (Corning SMF28-e) is slid into the bore hole of the ferrule and glued [Fig. 2.1(vii)]. At the opposite end, the fiber is plugged to a commercial optical interferometer readout (LDM1300, Attocube AG) that couples a laser source into the fiber and measures the amplitude of the signal reflected by the head of the probe [9, 15] This signal is the result of the interference between the light reflected at the fiber-to-gap interface, the light reflected by the gap-to-cantilever interface, and the light reflected at the cantilever-to-metal interface, and its amplitude is given by [9, 15]

$$W(d) = W_0\left[1 + V\cos\left(\frac{4\pi d}{\lambda} + \varphi_0\right)\right] \tag{2.1}$$

here d is the separation between the fiber-to-gap and the gap-to-cantilever interfaces, φ_0 is a constant phase shift that only depends on the geometry of the cantilever, λ is the wavelength of the laser (λ = 1310 nm), and W_0 and V are, respectively, the midpoint interference signal and the fringe visibility.

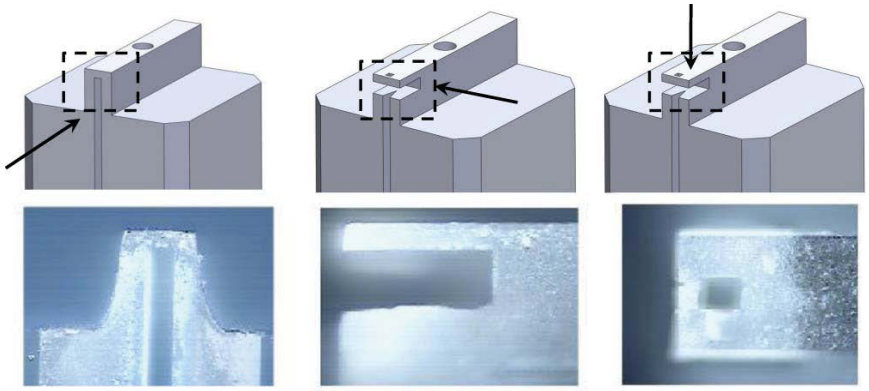

Fig. 2.2 Optical microscope images of the v-groove and of the suspended rectangular hole carved to host a ≈50 μm diameter fiber. The arrows in the drawings indicate the view direction.

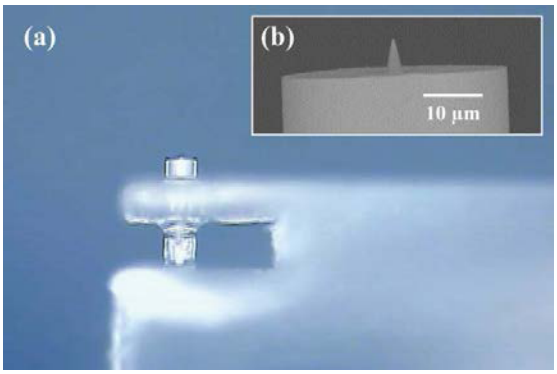

Fig. 2.3 (a) Optical microscope image of the end of the ridge after step (iv) of Fig. 1. (b) Scanning electron microscope image of the sharp tip formed on the GeO2 doped silica fiber by means of chemical etching in a buffered HF solution.

From the signal of the readout system, it is thus possible to remotely sense mechanical displacements of the ferrule-top device [9, 10, 12, 13]. It is to note that the fabrication procedure presented here is slightly different with respect to that described in Refs. 12 and 13. In the latter, the central fiber is glued before any carving procedure. In this way, however, the surface roughness of the fiber-to-gap and gap-to-cantilever interfaces is determined by the laser ablation process, which cannot provide optically smooth surfaces.

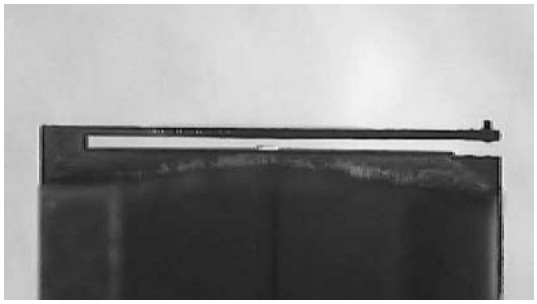

Fig. 2.4 Optical microscope image of a tipped ferrule-top cantilever.

The method described here, on the contrary, allows one to rely on optically smooth surfaces at all interfaces, increasing the fringe visibility. Thanks to this expedient, it is now possible to systematically achieve a root-mean-square (rms) deflection sensitivity on the order of 0.1 nm (and, thus, 0.3 nN rms force sensitivity for loads applied to the free hanging end of the cantilever) over the 35 kHz bandwidth of the interferometer.

2.3 EXPERIMENTAL SETUP

To demonstrate the imaging capabilities of ferrule-top cantilevers, the probe described in the previous section was mounted on the setup sketched in Fig. 2.5, which consists of a Z positioner (ANPz51/RES, Attocube AG) with a sample holder, mounted on a 30 μm × 30 μm range XY-scanner (ANSxy50, Attocube AG) in front of a ferrule-top probe holder equipped with a piezoelectric actuator (AE0203D04F, Thorlabs Inc.). The Z-positioner can be used in stick-slip mode (which moves the sample in discrete steps) or as a standard piezoelectric translator (which allows continuous displacement).

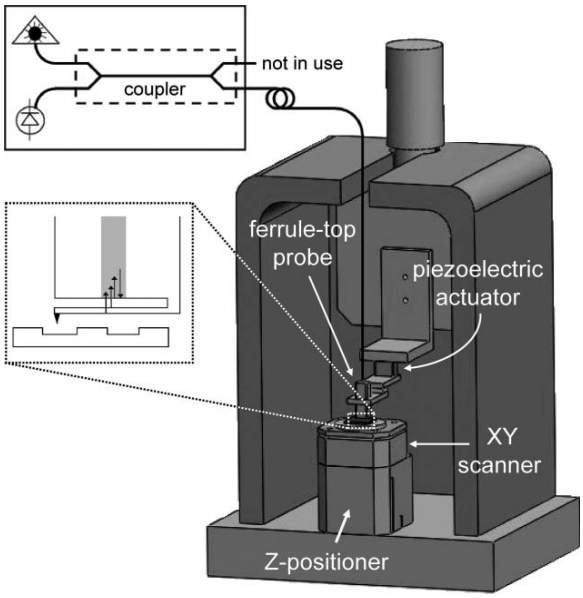

Fig. 2.5 Schematic view of ferrule-top AFM.

To facilitate assembly, the probe is glued to a thin 5 mm × 10 mm iron plate, which is anchored to the holder by means of a small magnet. To reduce acoustic and seismic noise, the entire assembly is mounted on an active vibration isolation stage (Nano-20, Accurion GmbH) housed inside an anechoic box. Thanks to the combined use of ferrule-top technology and compact scanners and positioners, the whole AFM can be contained in a 5 cm × 5 cm × 7 cm volume, and, with an accurate design, can be miniaturized even further.

2.4 CONTROL SYSTEM

To obtain a contact mode image, the operator first moves the Z-positioner in a series of discrete stick-slip steps that bring the sample in contact with the sharp conical tip of the ferrule-top cantilever. This procedure is extremely simple, because upon contact, the cantilever undergoes static bending, which is readily detected by the interferometer. Once in contact, the XY-scanner moves the sample underneath the tip to allow raster scan of the area of interest, while a feedback circuit keeps the cantilever deflection constant by moving the sample in the vertical direction, like in standard close loop AFMs.

To close the loop, one could simply fix the set point in correspondence to a position where the cantilever is in quadrature, and then adjust the vertical position of the sample to keep the output signal of the interferometer constant. Following this method, however, the image might be affected by spurious features that are caused by power fluctuations of the laser of the interferometer, which would give rise to signals that would mimic cantilever deflections. This systematic effect can be avoided by using a different feedback method designed to lock the set point not to quadrature but to a maximum or a minimum of interference. In this way, the set point is not defined in terms of absolute voltage output of the interferometer, but as the position where the first derivative of the signal vanishes, which is independent from the output power of the laser.

To lock to a maximum or a minimum of interference, the probe is sinusoidally excited in the vertical direction by means of the piezoelectric actuator of the probe holder at a frequency below the resonance frequency of the cantilever (like in some force modulation techniques already described in the literature) [16]. The amplitude of the oscillation is much smaller than the static bending of the cantilever at the set point. Therefore, the tip never loses contact with the surface. This vertical motion is at the heart of the feedback loop that eventually allows one to obtain accurate images of the sample, as explained in detail here below (see Fig. 2.6).

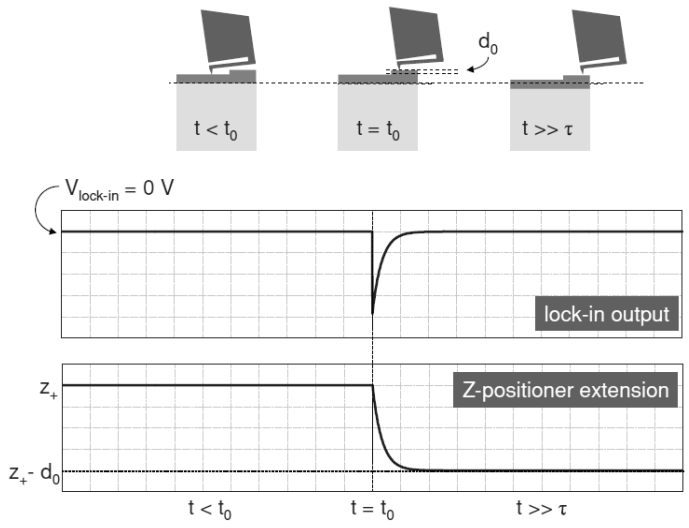

Fig. 2.6 Schematic view of the working principle that lies at the heart of the high gain feedback loop used in our ferrule-top AFM.

Let's suppose that, after contact, the Z-positioner, now working in piezoelectric scanning mode, is extended over a length equal to z_+ for which the interference signal is maximum. Let's then assume that the excitation

signal of the probe holder is switched on and that, during the XY-scan, the probe initially moves on a flat surface (no change of the output signal). Let's finally imagine that at $t = t0$ the cantilever is bent upward (or downward) of a small amount $d0$ because of the presence of a step in the sample. If one neglects the inertia of the cantilever and the rising time of the readout, the output signal observed is described by [see Eq. (2.1)].

$$W(t) \approx W_0(1+V) - \frac{1}{2} W_0 V \left(\frac{4\pi}{\lambda}\right)^2 \times \left(d_0 - z_+ + \delta\cos(\omega t)\right)^2 \qquad (2.2)$$

where ω and δ are, respectively, the angular frequency and the modulation amplitude of the cantilever in response of the oscillation of the probe holder. From Eq. (2.2), one can see that W is the sum of one time independent term, one 1ω term, and one 2ω term.

$$W(t) \approx C_0 + C_1(d_0)\cos(\omega t) + C_2\cos(2\omega t) \qquad (2.3)$$

where the exact expressions of C_0 and C_2 are not relevant for the description of the method, and $C_1(d_0)$ is given by

$$C_1(d_0) = W_0 V \left(\frac{4\pi}{\lambda}\right)^2 (d_0 - z_+)\delta \qquad (2.4)$$

To close the loop, the readout output is sent to a lock-in amplifier locked at frequency ω. The output of the lock-in amplifier is further amplified and sent to the power supply of the Z-positioner. The extension of the Z-positioner at a generic instant t is thus equal to

$$z(t) = \frac{G}{G+1}\left(z_{+} - d_0(1 - e^{-(t-t_0)/\tau})\right) \tag{2.5}$$

where G is the loop gain and τ is the loop time constant. From Eq. (2.5), it is evident that with sufficiently high gain one can accurately reconstruct the image of the sample by looking at the extension of the Z-positioner as a function of the XY-coordinate, and that, in principle, high speed rates can be achieved if the time constant is sufficiently low.

In our instrument, the loop gain and the time constant are set to 80 and 135 μs, respectively. However, we observed that, when driven at high frequencies, our Z-positioner suffers from severe mechanical oscillations that decrease the image quality. For this reason, we have intentionally limited the maximum output current of the amplifier that feeds the Z-positioner. This expedient decreases the scanning speed, but eliminates all the mechanical problems. For example, in Fig. 2.7 we show the movement of the Z-positioner in response to a driving signal that simulates a ≈25 nanometer sharp step. From that graph one can see that, indeed, the positioner does not suffer from mechanical oscillations. The response time is, however, limited by a 15 ms long rising time and a 10 ms falling time.

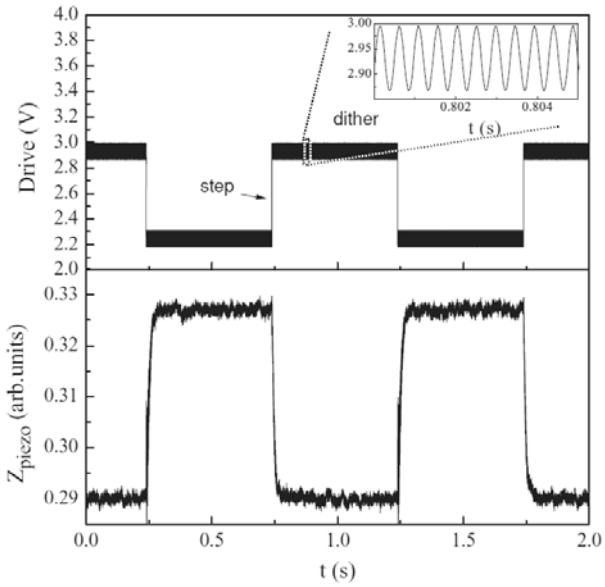

Fig. 2.7 Movement of the Z-positioner in response to a driving signal that simulates an ≈25 nm sharp step.

2.5 CONTACT MODE IMAGING

In Figs. 2.8(a) and 2.8(b) we report images of a 23 nm high calibration grating (NT-MDT TGZ1) obtained in air and water, respectively. For the latter, the grating was attached to the bottom of a small Petri dish filled with water. Each image covers an area of 7 μm × 4 μm (resolution 120 pixels × 70 pixels) with scan time of ≈12 minutes. The two images were obtained with two different cantilevers, whose resonance frequencies in atmospheric conditions were independently determined to be 4.9 kHz and 6.2 kHz, respectively. Those values correspond to spring constants of approximately 8 N/m and 15 N/m. Since the feedback mechanism needs, in the worst case

scenario, a cantilever deflection of λ/4 to engage at a maximum or a minimum of interference, the force applied onto the sample during the scan was anyway less than 7.2 μN and 13.5 μN, respectively. The frequency of the vertical oscillation that lies at the heart of the feedback loop was set to 1.1 kHz, with amplitude equal to 15 nm in air and 35 nm in water.

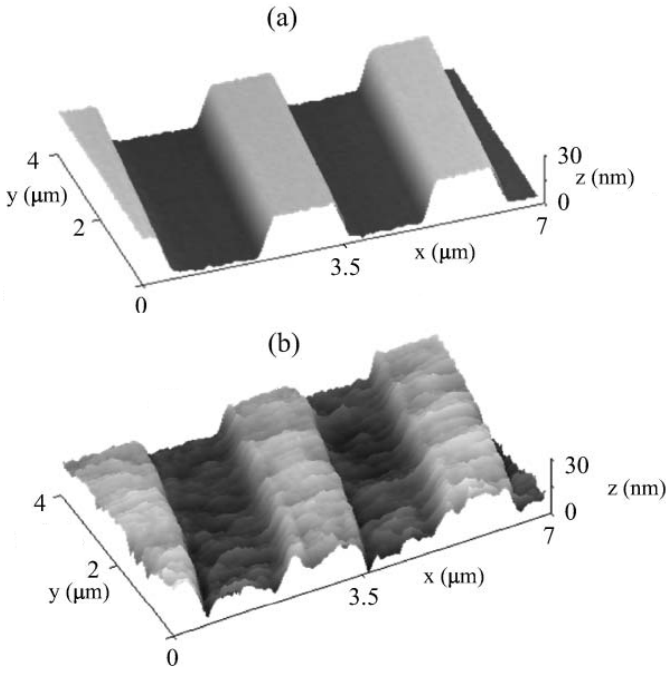

Fig. 2.8 AFM images of a calibration grating obtained with our ferrule-top AFM in (a) air and (b) water. Images were processed using Gwyddion software with implementation of only standard plane leveling and line correction (see Ref. 17).

From the images reported in Figs. 2.8(a) and 2.8(b), it is clear that the instrument can correctly reproduce the shape of the calibration grating. The line-scans reproduced in Fig. 2.9 further confirm that the quality of the image is comparable to that of commercial AFMs.

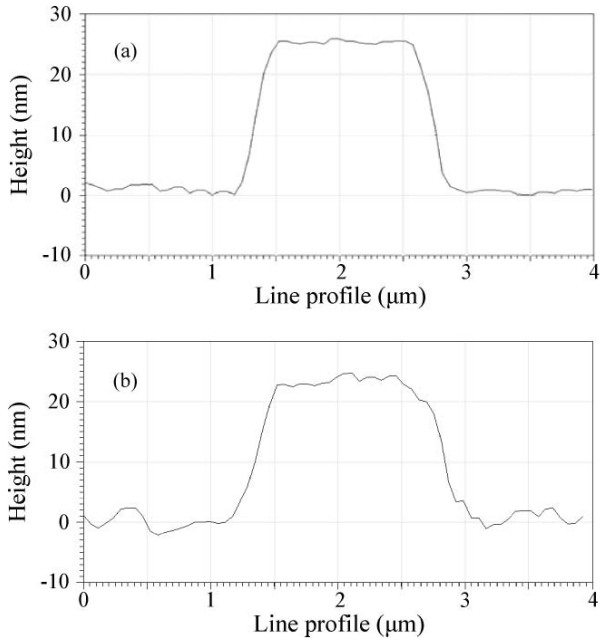

Fig. 2.9 Line-scan of the AFM images reported in Fig. 2.8: (a) in air, (b) in water.

Indeed, by analyzing the data recorded while the probe was scanning a flat region of the sample, one can see that the rms of the data distribution (that include the effects of vibrations and surface roughness) is equal to 0.5 nm for the image in air and 1.8 nm for the image in water. The slightly higher value obtained in water can be attributed to the presence of small turbulence around the probe, which increases vibrations and, therefore, noise.

2.6 CONCLUSIONS

We have fabricated a tipped ferrule-top cantilever for AFM purposes. We have demonstrated that this new kind of probe allows the implementation of very compact, all-optical, triangulation-free AFMs. Thanks to the monolithic design of ferrule-top technology, the user can quickly engage the scanning tip, regardless of the environment in which the sample is immersed. The instrument can then provide high quality images in both air and liquids. We believe that our work paves the way for a new generation of AFMs that are very easy to use, and thus adapt well to utilization in as well as outside research laboratories.

REFERENCES

[1] G. Binnig, C. F. Quate, and Ch. Gerber, Phys. Rev. Lett. 56, 930 (1986).

[2] O. Pfeiffer, R. Bennewitz, A. Baratoff, and E. Meyer, Phys. Rev. B65, 16403 (2002).

[3] T. Kasai, B. Bhushan, L. Huang, and C. Su, Nanotechnology 15, 731 (2004).

[4] Y. Su, A. Brunnschweiler, A. G. R. Evans, and G. Ensell, Sensors Actuators A76, 139 (1999).

[5] G. Schitter, P. Menold, H.F. Knapp, F. Allgower, and A. Stemmer, Rev. Sci. Instrum. 72, 3320 (2001).

[6] J. K. H. Horber, and M. J. Miles, Science 302, 1002 (2003).

[7] J. P. Howard-Knight, and J. K. Hobbs, Appl. Phys. Lett. 93, 104101 (2008).

[8] R. Pedrak, Tzv. Ivanov, K. Ivanova, T. Gotszalk, N.Abedinov, I. W. Rangelow, K.Edinger, E. Tomerov, T. Schenkel, and P. Hudek, J. Vac. Sci. Tech. B21, 3102 (2003).

[9] D. Iannuzzi, S. Deladi, V. J. Gadgil, G. P. Sanders, H. Schreuders, and M. C. Elwenspoek, Appl. Phys. Lett. 88, 053501 (2006).

[10] D. Iannuzzi, S. Deladi, J. W. Berenschot, S. de Man, K. Heeck, and M. C. Elwenspoek, Rev. Sci. Instrum. 77, 106105 (2006).

[11] S. Deladi, D. Iannuzzi, V. J. Gadgil, G. P. Sanders, H. Schreuders, and M. C. Elwenspoek, J. Micromech. Microeng. 16, 886 (2006).

[12] G. Gruca, S. de Man, M. Slaman, J. H. Rector, and D. Iannuzzi, Meas. Sci. Technol. 2, 094033 (2010).

[13] G. Gruca, S. de Man, M. Slaman, J. H. Rector, and D. Iannuzzi, Proc. SPIE 7503, PDP07 (2010).

[14] To obtain the tip, we used the method described in T. Pangaribuan, K. Yamada, S. Jiang, H. Oshawa, and M. Ohtsu, Jpn. J. Appl. Phys. 31, 1302 (1992). The fiber was cleaved and immersed for 360 minutes in a buffered HF solution (NH4F : HF : H2O, 7 : 1 : 1 volume ratio), where, because of the different etching rate of the cladding and the core, the tip spontaneously forms. Our fibers, however, had a slight dip in the doping profile in correspondence of the most central part of the core. This detail did not allow us to produce tips with a radius smaller than 100 nm. Using a fiber with a uniform doping profile, though, one should be able to systematically produce 10 nm radius tips.

[15] D. Rugar, H. J. Mamin, and P. Guethner, Appl. Phys. Lett. 55, 2588 (1989).

[16] P. Maivald, H. J. Butt, S. A. C. Gould, C. B. Prater, B. Drake, J. A. Gurley, V. B. Elings, and P. K. Hansma, Nanotechnology 2, 103 (1991).

[17] http://mesh.dl.sourceforge.net/project/gwyddion/user-guide/2009-11-11/ gwyddion-user-guide-en-2009-11-11.pdf

Chapter 3

Scanning Probe Microscopy – II

In previous chapter we demonstrated scanning probe microscopy using ferrule-top cantilever probe in air and liquid environment. In this chapter we extend the capability of ferrule-top cantilever probe for imaging at low temperatures (12 K) and in tapping mode. We also demonstrate the adaptability of ferrule-top probe for integration into a high speed AFM scanner and successfully achieve imaging rates up to 2 frames per second.

Adapted from: "Ferrule-top atomic force microscope II – Imaging in tapping mode and at low temperature"
REVIEW OF SCIENTIFIC INSTRUMENTS 82, 046107 (2011)
D. Chavan, D. Andres and D. Iannuzzi

"Towards high speed ferrule-top atomic force microscope"
IFAC SYMPOSIUM ON MECHATRONIC SYSTEM 2013
P. Chang, D. Chavan, R. Paris, D. Iannuzzi and G. Schitter

3.1 FERRULE-TOP AFM: IMAGING AT LOW TEMPERATURE AND TAPPING MODE

In 2006, one of us (D.I.) and his collaborators introduced a miniaturized optomechanical transducers for remote sensing: the fiber-top cantilever [1]. In a fiber-top probe, the cleaved end of an optical fiber is carved in the form of a cantilever, whose mechanical deflection is then determined by coupling light from the opposite side of the fiber. Fiber-top cantilevers have been proven to provide a new platform for several applications, including gas sensing [2] refractive index measurements [3] and atomic force microscopy [4]. Unfortunately, fiber-top cantilevers are currently fabricated by means of a time consuming process that does not adapt well to series production (namely, focused ion beam milling [5]). This problem was solved at the beginning of 2010 by introducing a larger (but still compact and monolithic) device that retains the advantages of fiber-top technology without the burden of the fabrication costs: the ferrule-top cantilever [6, 7]. In a ferrule-top device, the cantilever is carved out of a ferruled optical fiber. Because the dimensions of a ferrule are much large than those of a fiber, ferrule-top cantilevers can be fabricated with a series of steps that adapt better to cost effective series production. In a previous chapter [8] we demonstrated that a ferrule-top probe, equipped with a sharp conical tip on its free hanging end, can be successfully used for atomic force microscope imaging in air and liquids. The study, which was conducted with a custom-made scanner, was limited to contact mode.

Here, we show that a ferrule-top cantilever, now mounted on a commercial atomic force microscope, can provide tapping mode images at both room and cryogenic temperature (12 K).

3.1.1 Probe Fabrication

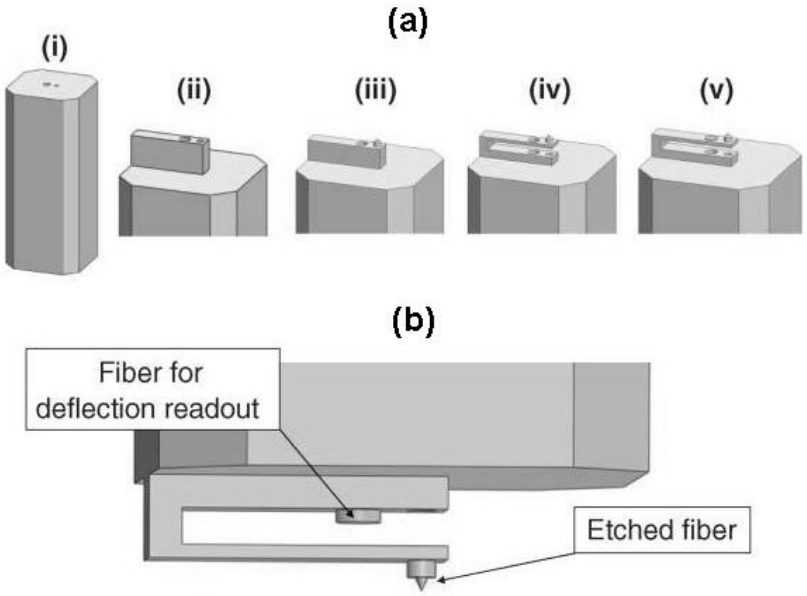

Fig. 3.1 (a) Illustration of the fabrication steps followed for the production of tipped ferrule-top cantilevers (not to scale): (i) the ferrule; (ii) fabrication of the ridge; (iii) assembly of the etched tipped fiber; (iv) fabrication of the undercut; (v) assembly of the readout fiber and filling of the remaining hole. The probe is eventually coated with a thin metallic layer (not illustrated). (b) Schematic view of a ferrule-top probe.

The ferrule-top cantilever used in this experiment was fabricated following a similar procedure as that described in Ref. 8 (see Figs 3.1 and 3.2). The building block is a 3 mm × 3 mm× 7 mm double-bore ferrule made out of borosilicate glass, which is carved in the form of a cantilever via laser

ablation. The two bore holes, with a diameter of 127 and 50 μm, are symmetrically positioned with respect to the central axis of the ferrule, with a center-to-center separation of 250 μm.

The smaller bore hosts a highly doped optical fiber, on top of which is a sharp conical tip obtained via differential wet etching [9, 10]. This fiber, which forms the tip for scanning, is glued into the bore before carving the undercut that frees the cantilever. The larger bore hosts a standard single mode optical fiber, which is glued into the ferrule only after the carving process is completed. The cleaved end of this fiber is kept well below the cantilever itself, and the hole left in the cantilever just above the fiber is filled with a droplet of UV curable epoxy. At the end of the process, the probe is mounted on a metal deposition system, where it is coated with a thin Cr+Au layer.

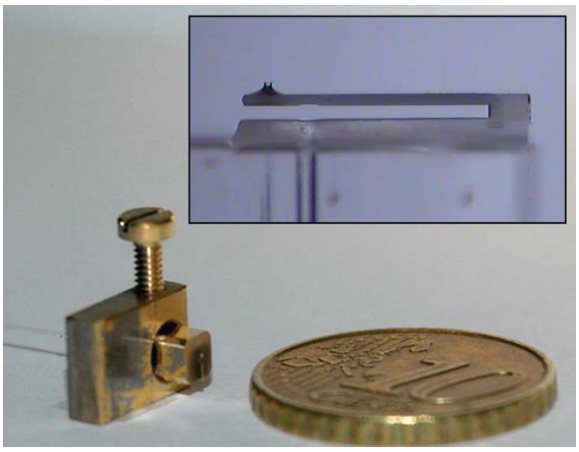

Fig. 3.2 Picture of a ferrule-top cantilever close to a 10 Eurocents coin.
Inset: Microscope image of a ferrule-top cantilever.

The cantilever used for the measurements presented here was 1600 μm long, 210 μm wide, and 30 μm thick with an expected spring constant of 20 N/m. The resonance frequency was measured using a frequency sweep the excitation piezo. The resonance frequencies measured at room temperature and at low temperature are shown in Fig. 3.3.

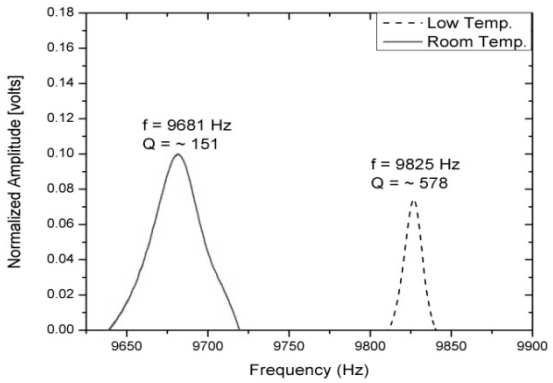

Fig. 3.3 Resonance frequency and Q-factor of ferrule-top cantilever at room temperature and low temperature (12 K).

As seen from the graph, the resonance frequency measured at room temperature (~9681 Hz) increases to (~9825 Hz) when the cantilever is at 12 K. The mechanical quality factor Q (calculated as the FWHM – full width half maximum) increases to 578 at low temperature as compared to 150 measured at room temperature.

3.1.2 Experimental Procedure

The ferrule-top probe was mounted on an AttoAFM Ixs atomic force microscope (Attocube Systems AG; for details, see Ref. 11). This instrument, which can operate down to a few millidegrees Kelvin , usually relies on standard cantilevers, which are held just below the cleaved facet of an optical fiber. Light from a laser coupled into the opposite end of the fiber allows interferometric detection of cantilever's deflections [12]. The wavelength of the laser (Pro8000 WDMsource, 1543 nm) can be adjusted to tune the optical cavity to quadrature. This readout system is very similar to the one used to measure cantilever's deflections in ferrule-top devices (see Refs. 6–8). With use of tunable laser source, one has greater flexibility in choosing the set-point for the feedback control and hence better contact force resolution while imaging in contact mode. One can thus plug the standard single mode optical fiber of the ferrule-top cantilever to the AttoAFM's readout system, mount the ferrule-top probe on the head of the instrument and set the instrument to work without any change of setup, electronics, computer program, or data analysis technique. The monolithic structure of our probe, which removes the burden of the fiber-to-cantilever alignment, simplifies the mechanical assembly of the cantilever, minimizes drifts, and eliminates the three motors that would be needed to align the fiber with the cantilever when standard probes are used. In Fig. 3.4, we report four images of a 20 nm high calibration sample (Anfatec AG, UMG01) obtained under different working conditions. The 200 × 200 pixels image reported in Fig. 3(a) and the 150 × 145 pixels image reported in Fig. 3(b) were obtained in air at room temperature using contact mode and tapping mode, respectively. The third 150 × 150 pixel image [inset (c)] was obtained in low pressure exchange gas atmosphere (5 torr) at 12 Kelvin using contact mode. The fourth image [inset (d)], which, because of the tendency of the substrate to accumulate electrostatic charges, is limited to 150 × 33 pixels, was obtained in vacuum at 12 K using tapping mode.

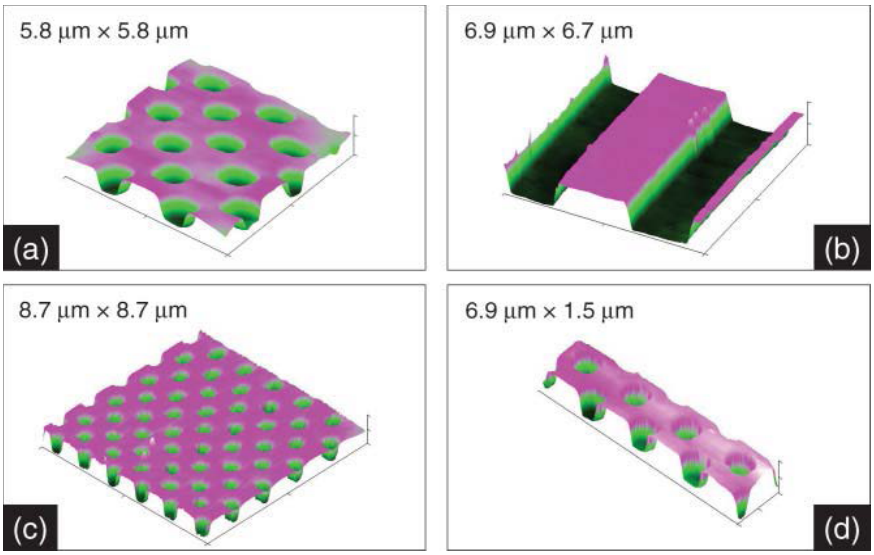

Fig. 3.4 (a) Atomic force microscope image of a 20 nm high calibration grating obtained with the ferrule-top cantilever operating in contact mode at room temperature. (b) Atomic force microscope image of a 20 nm high calibration grating obtained with the ferrule-top cantilever operating in tapping mode at room temperature. (c) Atomic force microscope image of a 20 nm high calibration grating obtained with the ferrule-top cantilever operating in contact mode at 12 K. (d) Atomic force microscope image of a 20 nm high calibration grating obtained with the ferrule-top cantilever operating in tapping mode at 12 K.

These measurements prove that ferrule-top probes can provide contact mode and tapping mode images of the same quality of those obtained with standard cantilevers, both at room and cryogenic temperatures. The ferrule-top probe also demonstrates the versatility of the device to adapt to any commercial AFM.

3.2 FERRULE-TOP HIGH SPEED AFM

The main drawback of the current AFM systems are the slow imaging speed and the complicated process of setting up the system, requiring alignment and adjustment of the AFM system by the user before each imaging experiment. In the last decade, considerable scientific activities have aimed at improving the speed of imaging. To improve the x-y raster movement, alternative physical scanner designs [13, 14, 15] as well as advanced control applications [16, 17, 18] have been reported. Other studies have also reported to provide faster control of the tip sample (z-measurement) force, such as [19, 20, 21]. In order to detect the tip/sample interaction, commercial AFM systems typically use an optical lever systems [22]. This method shines a laser beam onto the back of an AFM cantilever to measure the reflected beam by a split photodetector (see Fig. 1). However, this system requires manual adjustment, and takes certain space for its optical path. Thus recent AFM developments are also aimed towards the replacement of the optical lever detection, to bring ease of use and miniaturization to AFM systems. Electromechanical and thermo-mechanical cantilevers with an integrated detection have been proposed by [23] and [24]. However, these probes need electrical sources and are more complex to fabricate. Furthermore, they face limitation for operations in liquid environment, due to the need for isolation of the electric conductors. On other hand, a ferrule-top cantilever probes with its inherent all-optical design are self aligned, easy to use and present a unique tool for imaging at nanoscale [8].

In this work we have attempted to integrate a ferrule-top probe with a high-speed AFM scanner to address two major limitations of current AFM systems.

3.2.1 Probe Readout

The readout of ferrule-top cantilever probe records the deflection of the cantilever based on Fabry-Perot interferometry. The readout scheme used for the ferrule-top probe is similar to shown in previous chapter. An infrared laser is connected to an optic fiber coupler, wherein one arm is connected to the detection fiber and the other arm is not in use. The photodiode gives the intensity of the light reflected back from the cantilever. The initial photodiode output depends on the geometry of the probe and wavelength of the laser. Depending upon the measurement requirement and mode of imaging (contact mode or non-contact mode) one might need to tune the initial photodiode output to the desirable location on the interference fringe. At this point, the geometry of the probe is not a possible parameter to control, as the dimensions and gap distance d are fixed during fabrication. Hence, one can consider a tunable wavelength laser source for adjusting the initial photodiode output.

An interferometer based on a tunable source wavelength allows one to obtain an initial photodiode output at quadrature of the interference fringe for highest possible deflection sensitivity (nm/Volts). The tunable wavelength feature of the readout also offers a better force resolution for contact mode AFM imaging. For the present experiment, we use OP1550 (Optics11 B.V.) tunable wavelength source interferometer.

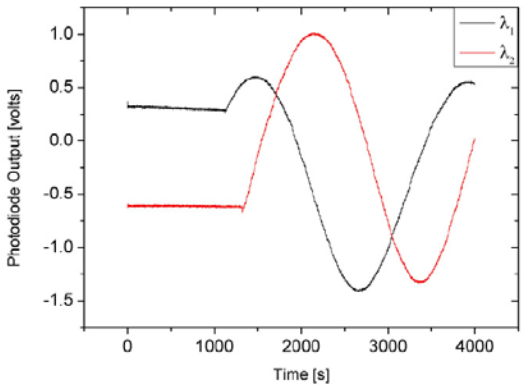

Fig. 3.5 Interferometer photodiode output comparison of two different wavelength.

The interferometer allows one to choose the wavelength from 1528 nm to 1563 nm with step of 0.8 nm. Fig. 3.5 shows the photodiode output obtained by two different wavelengths (λ_1 = 1528; λ_2 = 1557) nm, while the cantilever is pressed against the glass. As shown in Fig. 3.5, the initial photodiode output for wavelength λ_1 is not at quadrature of the interference fringe. Hence, one can selectively change the wavelength of source to λ_2, which has its initial photodiode output at quadrature of the interference fringe.

3.2.2 High Speed AFM Scanner

High speed AFM scanner enables XY raster scanning of a sample at rates few orders of magnitude higher than conventional AFM scanners. Details of the high speed AFM scanner design is described in [13], with an overview presented in this section.

The high speed AFM system is developed such that it allows scanning speeds that are three orders of magnitude faster than commercial AFM systems. The scanner has a z-piezo that is used for vertical positioning, mounted on a center piece moved by x-y piezos for lateral positioning (See Fig. 3.6). With a balanced and decoupling design that focuses on rigidity and compactness, this high speed scanner's x-axis has its dominant resonance frequency at 22 kHz, with a travel range of 13 μm. For AFM imaging operation, a small piece of sample is placed on top of the central z-piezo, and this sample is actively moved in a raster scanning pattern in the x-y plane by driving the lateral piezos. The command signal on the fast axis movement is typically open-loop operated. Input shaping was adapted to avoid exciting the resonance of the scanner, thus this scanner is able to achieve a raster scan with a line scan rate at 7.9 kHz [25]. As for the z-measurement part, this high speed AFM scanner is controlled by an analog Proportional-Integral (PI) feedback controller to maintain the tip/sample separation, through the extension and retraction of the z-piezo with respect to a set cantilever deflection. This measurement loop, takes the sample topography as a disturbance input, measured through the cantilever and deflection measurement block, and the PI controller's command signal is recorded as the topography profile.

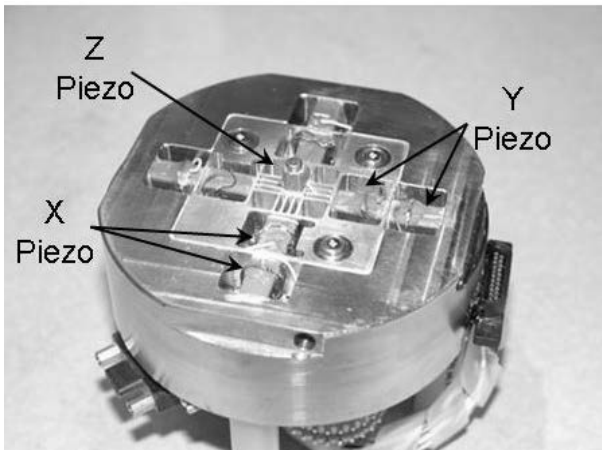

Fig. 3.6 High speed AFM scanner

From an AFM feedback system's point of view, the cantilever and deflection measurement block is replaceable with any physical device, as long as it provides an deflection measurement. Thus the ferrule-top cantilever probe readout system is integrated at this point.

3.2.3 System Integration

An adapter was designed in order to combine the ferrule-top probe with the high speed AFM scanner system, as shown in Fig. 3.7. The adapter is an L-shaped metal plate that attaches to a base plate magnetically. The adapter itself has a micrometer for coarse z adjustment, on which the ferrule-top probe is attached. The base plate has a central hole that exposes the scanner's z-piezo and sample, and is fastened through three adjustable support and allows fine z-direction movements. The compact adapter design places the

ferrule-top probe directly over the sample. At this point, the ferrule-top deflection output from the readout is connected to the feedback and the setpoint for the feedback is fixed for desired contact force while imaging. Hence, before the engagement of the tip with the sample, the z feedback piezo is fully extended. The base plate is lowered by the fine z-stage, which brings the probe in contact with the sample. The engagement procedure can be automated or done with manual intervention. The fine z movement is continued till the setpoint is reached.

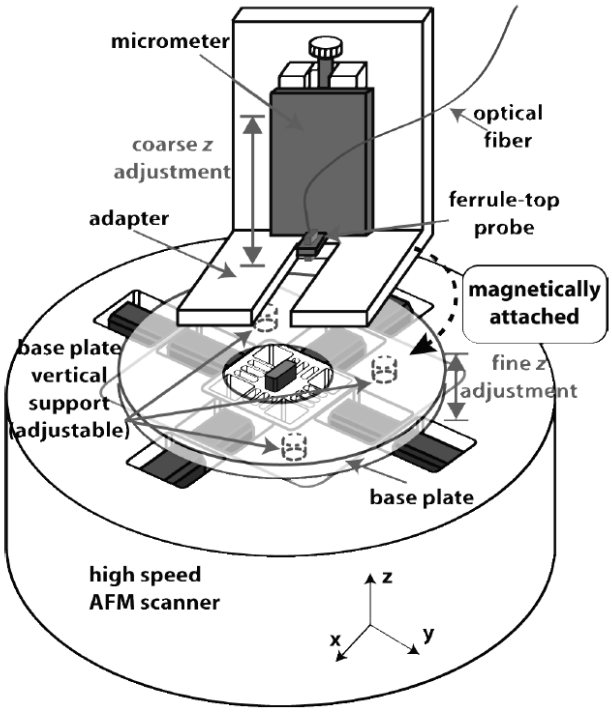

Fig. 3.7 Adapter design to integrate the ferrule-top probe with the high speed AFM scanner

Note that the deflection readout is directly feed into the analog PI-controller that controls the z-measurement feedback loop. The ferrule-top probe and its interferometer readout system directly replace the conventional optical lever system. With use of ferrule-top, the whole AFM deflection measurement head is compact and needs no laser alignment.

3.2.4 Experimental Results

Several different ferrule-top cantilevers were tested for high-speed AFM imaging. To ensure adequate sensitivity, the deflection readout has been adjusted according to the following example. Since the source laser wavelength is adjustable, one can tune the readout output to the desired position within the interference fringe. First a ferrule-top cantilever is intentionally pressed for examination on its readout response. This is achieved by driving the z-piezo with a triangular signal to move the sample up and down, while a ferrule-top probe is engaged with the sample surface. By examining the response from the press procedure, the readout is tuned. The desired adjustment goal is to place the deflection readout's linear response region around the AFM PI-controller set-point, so to ensure optimized sensitivity of the cantilever deflection signal. AFM imaging was performed on a standard AFM silicon calibration grating sample, which has a pitch size of 3 μm and a step size of 44 nm.

The results are shown in Fig. 3.8, showing height and deflection images scanned over the same area at different scan speeds. The area scanned is 5 μm by 5 μm in size. These images have a pixel resolution of 256 by 256 and are taken with the trace scanning direction (left to right). Fig. 3.8 (a) and (b) are recorded at a line scan rate of 514 Hz, (c) and (d) at 257 Hz, and (e) and (f) were imaged at 128 Hz. These scan rates corresponds to 0.5, 1, and 2.0 frames per second respectively. The analog PI feedback controller for controlling the cantilever deflection was manually tuned to obtain the best imaging results. It can be observed that at a higher scan speed (b), ringing effects from the deflection images are more pronounced, as compared to the

two slower scan images ((d) and (f)). This is due to the fact that the ferrule-top cantilever resonance of 13 kHz is excited as it crosses over the grating edge. This resonance behavior is also evident in the deflection cross-sectional profiles shown in Fig. 3.9.

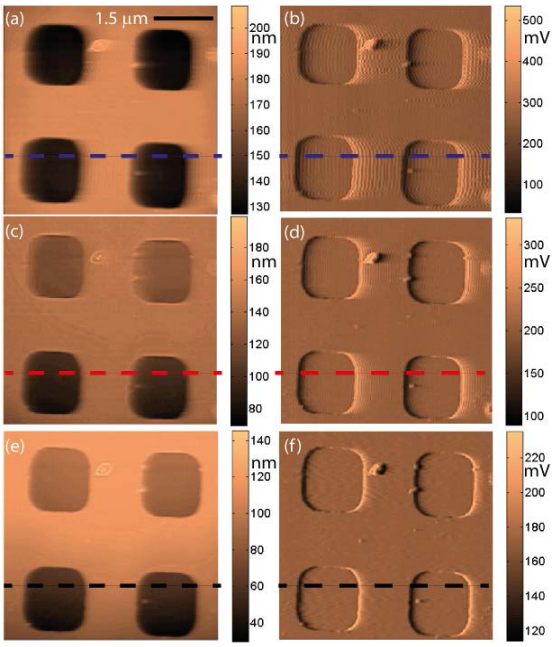

Fig. 3.8 Height (left) and deflection (right) scans at different scan speeds.

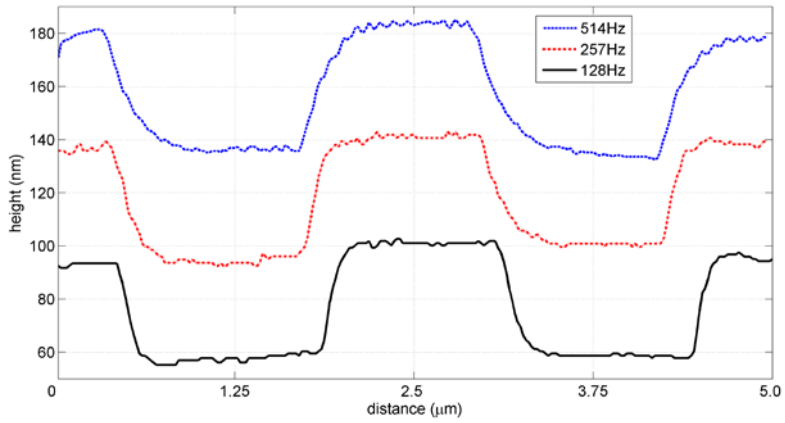

Fig. 3.9 Height line scan at different line scan speed.

Line scan profiles shown in Fig. 3.9 are taken from the image location as indicated by the dashed-lines in Fig. 3.8. Fig. 3.9 clearly shows the profile of the grating with an width of 1.5 μm and a 44 nm step height. As mentioned earlier, this resonance is excited from the step change from the grating, which is not observed from the surface, as evident from the deflection images earlier. The oscillation is measured for 10 pixels from the data, corresponding to a resonance frequency of 13:11 kHz. Using appropriate selection of the PI-controller parameter, this oscillation can be avoided in the height measurement, thus maintaining height measurement with negligible oscillations. These imaging result shows that it is possible to use a ferrule-top cantilever with a higher resonance frequency, to utilize the full potential of the described high-speed AFM scanner, and increase the imaging speed to even higher frame rates.

3.3 CONCLUSIONS

In two different experimental setups and conditions, we demonstrated the capability of ferrule-top cantilever probe for nanoscale imaging. This emphasizes the usability of ferrule-top for fundamental research at low temperatures and at the same time possibility to develop an industrial solution for nanoscale characterization. These experiments also highlight the high degree of adaptability of the probe to commercial and non-commercial scanning probe microscopy systems.

REFERENCES

[1] D. Iannuzzi, S. Deladi, V. J. Gadgil, G. P. Sanders, H. Schreuders, and M. C. Elwenspoek, Appl. Phys. Lett. 88, 053501 (2006).

[2] D. Iannuzzi, S. Deladi, M. Slaman, J. H. Rector, H. Schreuders, and M. C. Elwenspoek, Sens. Actuators B 121, 706 (2007).

[3] C. J. Alberts, S. de Man, J.W. Berenschot, V. J. Gadgil, M. C. Elwenspoek, and D. Iannuzzi, Meas. Sci. Technol. 20, 034005 (2009).

[4] D. Iannuzzi, S. Deladi, J. W. Berenschot, S. de Man, K. Heeck, and M. C. Elwenspoek, Rev. Sci. Instrum. 77, 106105 (2006).

[5] S. Deladi, D. Iannuzzi, V. J. Gadgil, G. P. Sanders, H. Schreuders, and M. C. Elwenspoek, J. Micromech. Microeng. 16, 886 (2006).

[6] G. Gruca, S. de Man, M. Slaman, J. H. Rector, and D. Iannuzzi, Meas. Sci. Technol. 21, 094033 (2010).

[7] G. Gruca, S. de Man, M. Slaman, J. H. Rector, and D. Iannuzzi, Proc. SPIE 7503, PDP07 (2010).

[8] D. Chavan, G. Gruca, S. de Man, M. Slaman, J. H. Rector, K. Heeck, and D. Iannuzzi, Rev. Sci. Instrum. 81, 123702 (2010).

[9] T. Pangaribuan, K. Yamada, S. Jiang, H. Oshawa, and M. Ohtsu, Jpn. J. Appl. Phys. 31, 1302 (1992).

[10] In Ref. 8, we made use of a single bore glass ferrule where we first ablated a v groove to accommodate the etched fiber. The use of custom made doublebore glass ferrules eliminates the fabrication of v-groove, and thus further simplifies the fabrication process.

[11] http://www.attocube.com/nanoSCOPYxs/afmIxs.htm.

[12] D. Rugar, H. J. Mamin, and P. Guethner, Appl. Phys. Lett. 55, 2588 (1989).

[13] G. Schitter, K. J. Astrom, B. E. DeMartini, P. J. Thurner, K. L. Turner, and P. K. Hansma, IEEE Trans. Control Syst. Technol. 15, 906 (2007).

[14] T. Ando, T. Uchihashi, and T. Fukuma, Prog. Surf. Sci, 83, 337 (2008).

[15] K. K. Leang, and A. J. Fleming, Asian J. Control, 11, 144 (2009).

[16] G. Schitter, and A. Stemmer, Microelectron. Eng. 67-8, 938 (2003).

[17] A. Sebastian, and S. M. Salapaka, IEEE Trans. Control Syst. Technol. 13, 868 (2005).

[18] G. M. Clayton, S. Tien, A. J. Fleming, S. O. R. Moheimani, and S. Devasia, Mechatronics 18, 273 (2008).

[19] G. Schitter, P. Menold, H. F. Knapp, F. Allgower, and A. Stemmer, Rev. Sci. Instrum. 72, 3320 (2001).

[20] D. R. Sahoo, A. Sebastian, and M. V. Salapaka, Appl. Phys. Lett. 83, 5521 (2003).

[21] S. Kuiper, and G. Schitter, Mechatronics 22, 327 (2012).

[22] G. Meyer, and N. M. Amer, Appl. Phys. Lett. 53, 1045 (1988).

[23] U. Drechsler, N. Burer, M. Despont, U. Durig, B. Gotsmann, F. Robin, and P. Vettiger, Microelectron. Eng. 67-8, 397 (2003).

[24] T. Akiyama, U. Staufer, and N. F. de Rooij, Appl. Surf. Sci. 210, 18 (2003).

[25] G. Schitter, P. J. Thurner, and P. K. Hansma, Mechatronics 18, 282 (2008).

Chapter 4

Scanning Probe Microscopy – III

In this chapter, we demonstrate the potential of fiber-top and ferrule-top cantilever probes to simultaneously probe sample topography and collect/emit light at the nanoscale. We discuss here the experimental details and advantages/disadvantages of the new probe over the conventionally used near field microscopy techniques.

Adapted from: "Fiber-top atomic force microscope probe with optical near field detection capabilities"
JOURNAL OF MICROSCOPY 242, 10 (2011)
B. Tiribilli, G. Margheri, P. Baschieri, C. Menozzi, D. Chavan and D. Iannuzzi

"Fiber-top and ferrule-top cantilevers for atomic force microscopy and scanning near field optical microscopy"
OPTICAL MICRO- AND NANOMETROLOGY IV, SPIE PROCEEDINGS 8340, (2012)
D. Chavan, G. Gruca, T. van de Watering, K. Heeck, J. Rector, M. Slaman, D. Andres, B. Tiribilli, G. Margheri and D. Iannuzzi

4.1 FIBER-TOP AFM PROBE FOR NEAR FIELD DETECTION

4.1.1 Introduction

Scanning Near-field Optical Microscopy (SNOM) [1,2] is widely recognized as an invaluable tool for the investigation of optical phenomena beyond the diffraction limit, with applications that range from single molecule spectroscopy to the analysis of complex biological systems [3]. In most of those applications, to achieve ultimate resolution the instrument needs a feedback system that controls, with nanometer precision, the separation between the tip that collects the near-field and the surface under investigation. Most SNOM microscopes currently achieve this goal by monitoring the dynamical response of the probe in response to a vertical (tapping-mode feedback) or horizontal (shear-force feedback) excitation. In techniques using tuning forks, an etched (or pulled) optical fiber is glued to a tuning fork. The tuning fork has an excitation electrode to excite it at resonance frequency and a readout mechanism to monitor the shift in resonance frequency. As the optic fiber glued to the tuning fork approaches the sample surface, it experiences surface forces that cause a shift in its resonance peak. This shift is related to the distance from the surface, and can be used as feedback signal to maintain a constant distance from the sample surface. The feedback control system in this technique demands high quality factor to maintain the close loop while scanning. As a result, it becomes challenging to image samples in liquid, as the viscous damping causes drop in quality factor and makes it difficult for control system to close the loop. Hence the tuning fork technique is not suitable for imaging in liquid. Also the shear force mode operation of tuning fork puts limitation on the speed of scanning. Alternatively, one can bring the tip in contact with the surface and, while scanning in the horizontal direction, keep the force acting on the tip constant (contact mode). To monitor the oscillations of the tip or the force acting onto it, one generally uses either the optical triangulation readout of an atomic force microscope (AFM) [4, 5] or the piezoelectric

signal coming from a tuning fork to which the probe is solidly attached [6]. Optical triangulation requires bulky readout components. Furthermore, its utilization is complicated by the alignment procedure needed to close the optical path from the laser source to the quadrant detector. The tuning fork expedient, by contrast, does not adapt well to liquid environments. It is thus clear that an SNOM probe that could rely on AFM cantilevers without the burden of the optical triangulation would represent a significant step ahead.

In 2001, Minh *et al.* [7] circumvented the problem by gluing a cantilever on top of an optical fiber. Coupling light into the fiber, one can assess whether the tip is in contact with the sample or not. The SNOM signal scattered at the tip, amplified by a glass ball lens, is then collected on a photomultiplier located in the proximity of the surface. A few years later, one of us (DI) and his collaborators showed that one can obtain a monolithic cantilever probe with optical readout by carving a thin rectangular mechanical beam from the cleaved end of an optical fiber [8]. Light coupled from the opposite end allows the user to precisely determine the deflection of the cantilever in response to an external force, and, thus, to directly measure that force. The device, which goes under the name of fiber-top cantilever, has been already proven to be an interesting alternative for the implementation of all-optical, miniaturized, triangulation-free AFM microscopes [9], and thus represents a potential candidate to solve the problem described earlier.

Here, we show that fiber-top cantilevers equipped with a sharp central tip and mounted on a detection system similar to what earlier proposed in a more conventional AFM-based SNOM microscope [10] can indeed be used to detect the evanescent optical field emerging from a prism illuminated under total internal reflection conditions. Simultaneously, the light coupled from the opposite end of the fiber can still provide information on the position at which the tip of the cantilever enters into contact with the prism.

4.1.2 Fiber-top AFM Probe Fabrication

The AFM-SNOM fiber-top probe presented here was fabricated following the steps indicated in Fig. 4.1 [11]. A single mode optical fiber is stripped of its jacket, cleaved, coated with a 50nm Au layer, and mounted vertically inside a focused ion beam milling machine. After setting the beam energy to 30 keV and the beam current to 20 nA, the end of the fiber is machined in the form of a rectangular ridge (Fig. 4.1 A). The fiber is then rotated of 90° with respect to the ion beam direction, where, using a 7 nA beam current, it is carved to reduce the length and, partially, the thickness of the ridge (Fig. 4.1 B). The residual block at the end of the ridge, just above the core, is further machined in the form of a sharp pyramidal tip (Fig. 4.1 C). Each facet of the pyramid is obtained after proper adjustment of the milling angle (always 45◦ with respect to the direction of the ion beam) and with a 1 nA beam current. With the fiber back in the orthogonal position, the beam current is then increased to 3 nA to open a square undercut in the ridge and free the cantilever from the body of the fiber (Fig. 4.1 D). To facilitate the approach of the probe to the sample during SNOM and AFM experiments, large part of the fiber is finally removed from the edge opposite to the anchor point of the cantilever (Fig. 4.1 E; milling parameters: 20 nA beam current, 45◦ angle). Fig. 4.1 F shows a scanning electron microscope image of the device at the end of the fabrication process.

The cantilever is ≈60 μm long and ≈13 μm wide, and its thickness ranges from ≈1.6 μm (close to the base) to ≈2.5 μm (close to the free hanging end), with an expected spring constant on the order of 10 N/m (i.e. similar to that of standard tapping mode cantilevers). The gap between the cantilever and the rest of the fiber is ≈2 μm. The ≈13 μm × 13 μm × 8 μm pyramidal tip has an apex curvature radius of approximately 200 nm, which is larger than that typically achieved with pulled fiber tips [12] or chemically etched fibers [13, 14, 15]. It should be however possible to carve sharper tips by lowering the current during the milling process or by combining the etching method described in [16] with the carving approach proposed in [8] and used in this paper.

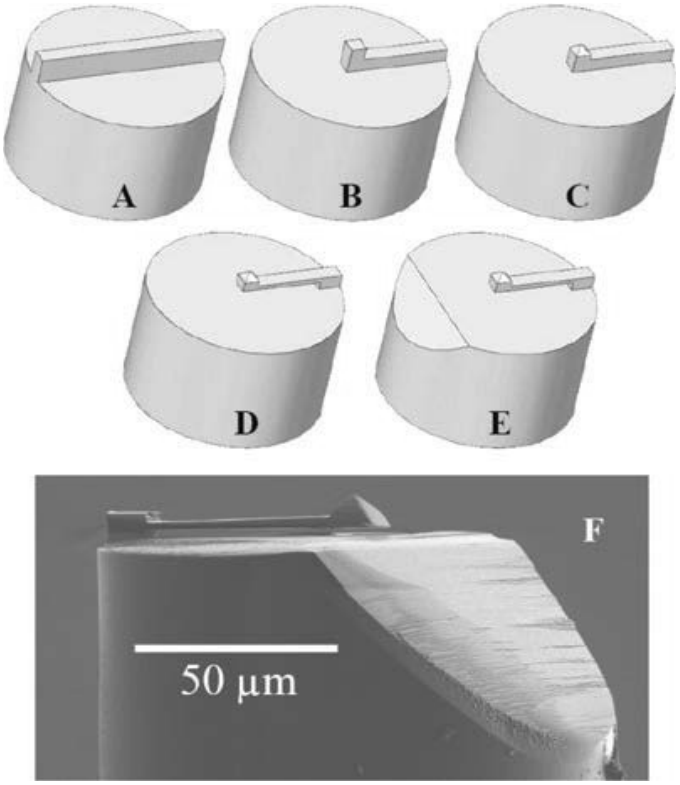

Fig. 4.1 (A–E) Milling steps followed to carve a fibre-top AFM-SNOM probe out of the cleaved end of a single mode (not to scale). (F) Scanning electron microscope image of a fibre-top AFM-SNOM probe.

4.1.3 Experimental Setup

The AFM-SNOM probe was mounted in the experimental setup sketched in Fig. 4.2. An optical prism is fixed to the sample holder of a custom made AFM on top of a tri axial translational stage (Piezosystem Jena–Tritor 38, Germany) equipped with strain gauge position sensors and linearization system to compensate piezoelectric hysteresis. The fiber-top probe is positioned on a vertical stage in front of the translator with the cantilever at a 12 degree angle with respect to the top surface of the prism. A 532 nm, 20 mW laser beam (WSTech, Canada) is shone inside the prism at an incident angle higher than the critical angle of the glass–air interface, thus generating an evanescent electromagnetic field just outside the top surface of the prism. The evanescent field, which represents the SNOM signal, can be then collected by the pyramidal tip of the fiber-top cantilever and guided through the fiber up to the opposite end.

To measure the SNOM signal and still maintain the possibility to detect cantilever deflections with another independent optical readout, the fiber is connected to a 50/50 optical fiber coupler whose output branches are respectively coupled to a photomultiplier (Hamamatsu 9306-03, Japan) for the detection of the 532 nm SNOM signal and to a commercial optical fiber interferometer (Attocube ARP100, Germany). The interferometer allows direct detection of the motion of the cantilever by sending an infrared laser light into the fiber (wavelength ≈1310 nm, output power ≈0.5 mW) and measuring the amplitude of the return signal (see ref. 8 for details). Note that, because the photocathode is not sensitive to infrared light, the return signal does not generate any signal on the photomultiplier.

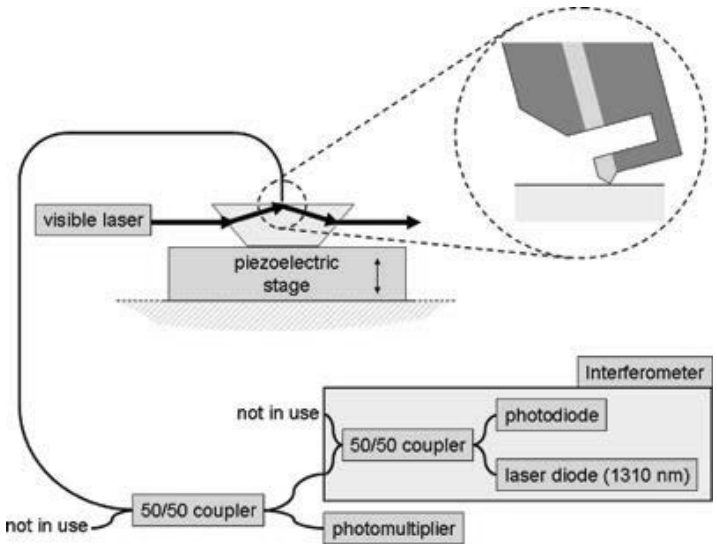

Fig. 4.2 Sketch of the experimental setup used to test the fiber-top AFM SNOM probe (not to scale).

4.1.4 Results And Discussion

To demonstrate that our fiber-top probe can both detect the SNOM signal and the mechanical deflection of the cantilever, the piezoelectric transducer was driven along the vertical axis by a 0.5 Hz, 100 mV peak-to-peak triangular signal, which corresponds to a 300-nm-long forward and backward linear motion. Adjusting the offset applied to the piezoelectric translator, we made sure that the cantilever tip entered into contact with the prism during the forward sweep and jumped out of contact during the backward retraction. Fig. 4.3 shows the output signal of the photomultiplier and of the interferometer observed during the experiment. During the forward motion, the photomultiplier signal increases exponentially up to a certain point, after which it remains constant. The exponential signal corresponds to the near-field in the proximity of the prism, whereas the flat signal indicates that the probe is in contact with the surface. At the same

time in which the photomultiplier signal flattens, in fact, the interferometer signal sharply increases. With further forward motion, the interferometer signal decreases. The first sharp increase can be ascribed to the jump-to-contact deflection of the cantilever, where the cantilever moves towards the prism and away from the fiber under the influence of surface attractive forces. Once the tip is engaged, vertical movements of the prism make the cantilever move towards the fiber, giving rise to a decrease of the interferometer signal. The signals corresponding to the backward movement of the piezoelectric translator are, as expected, the specular image of those observed during the forward movement, with the exception of the points close to the pull-out instant, where the cantilever undergoes a large outward deflection before it can overcome the capillary force that keeps the tip attached to the prism. As soon as the tip disengages the surface, the cantilever quickly moves back to its straight position, as clearly indicated by the sharp decrease of both the AFM and the SNOM signals. The smooth decrease of the interferometer signal observed at larger separation is an artifact due to some 1310 nm light that is not completely reflected by the probe and, after impinging on the prism, enters back into the fiber.

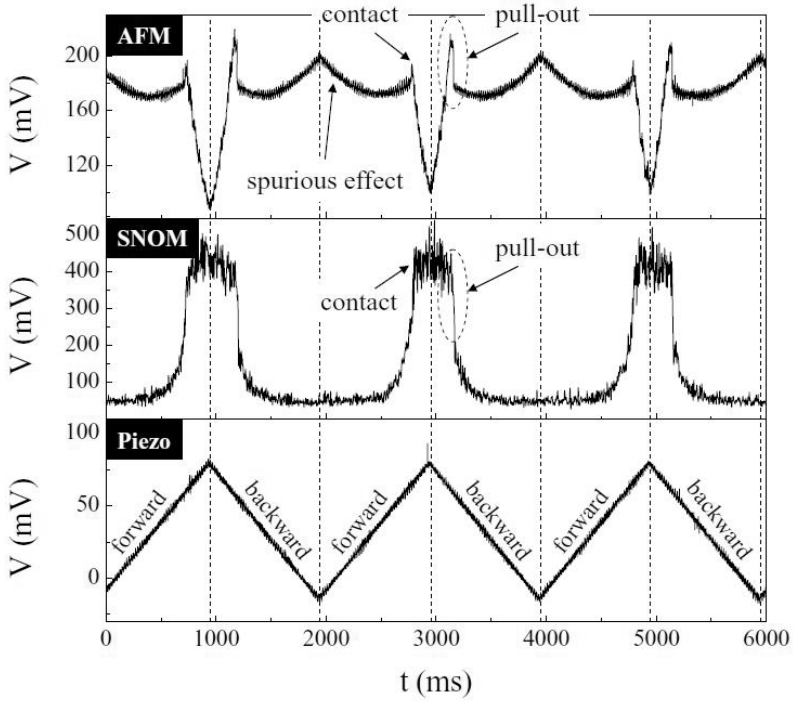

Fig. 4.3 Demonstration of the AFM-SNOM capabilities of the fiber-top probe developed for this experiment. Bottom graphic: output of the strain gauge sensor that measures the extension of the piezoelectric stage on which the sample is mounted. Central graphic: output signal of the photomultiplier (near-field). Top graphic: output signal of the interferometer (cantilever deflection). All graphics are plotted as a function of time, covering three consecutive forward–backward traces.

To further confirm that the signal detected by the photomultiplier corresponds to the light that tunnel from the prism into the probe, we coupled a tunable laser (Coherent Inc., Innova70, CA, USA; 1W maximum optical power) into the prism and verified whether the decay constant *d* of

the SNOM signal observed during the tip-to-prism approach is proportional to wavelength. For this analysis, we neglect the dependence of the refractive index of the prism on laser wavelength, which varies from 1.576 at λ= 488 nm to 1.571 at λ= 568 nm. In Fig. 4.4, we report the response of the photomultiplier observed in correspondence of λ = 488 and 568 nm. The graphs contain an elaboration of data recorded during 10 consecutive tip-to-prism approaches. The contact point of each run (z = 0) was determined from the analysis of the corresponding interferometer signal.

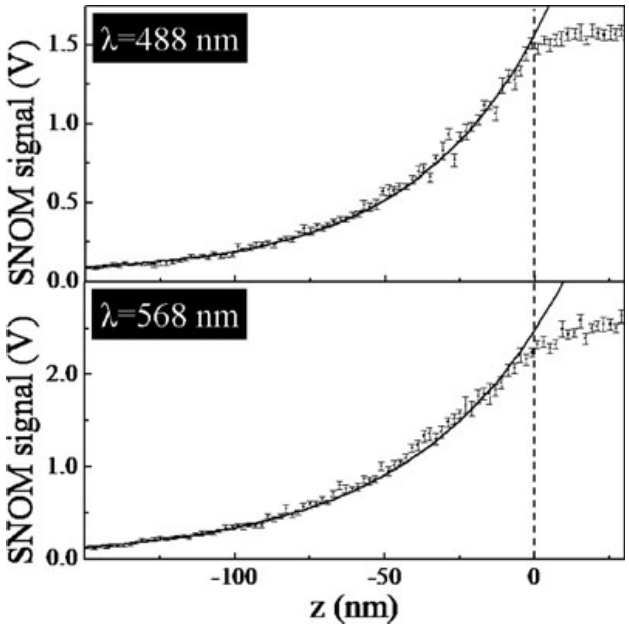

Fig. 4.4 Output signal of the photomultiplier (near field) as a function of time observed during then linear tip-to-prism approach. Data were elaborated as explained in the text. The top and bottom graphs correspond to the results obtained with evanescent field wavelength equal to 488 and 568 nm, respectively. The two continuous lines represent the best fit of the data with an exponential curve.

The tip-to-prism separation z was then retrieved via the signal recorded by the strain-gauge of the translational stage. All the data coming from the 10 runs were finally averaged with a binning width of 2 nm. Data in the distance range between –200 nm and 0 nm were fitted with an exponential curve of the kind $V = C + Ae^{z/d}$ (continuous lines of Fig. 4.4), where C, A and d are free parameters. Following standard χ^2 minimization procedures, one gets $d_{488} = 42.7 \pm 0.5$ nm for $\lambda = 488$ nm and $d_{568} = 49.9 \pm 0.7$ nm for $\lambda = 568$ nm, with an increase of 17 ± 2% in d in correspondence of a 16% increase in λ, in perfect agreement with what expected.

4.2 COMBINED AFM AND OPTICAL TRANSMISSION MICROSCOPY

4.2.1 Introduction

In previous section (4.1) we demonstrated the use of fiber-top cantilever probe for scanning near field optical microscopy. The fiber-top cantilever probe has the advantage of having a lower spring constant (compared to bend fiber). Furthermore, it requires no optical triangulation (unlike bent fibers) and can be operated in liquids. However, fiber-top cantilever probes are fabricated by focused ion beam milling, which makes them extremely expensive and time intensive to fabricate. On the other hand, ferrule-top cantilever probes are easy to fabricate and the tip that scans over the sample to provide topological information, can also be used simultaneously for collecting/emitting light while scanning. To encompass this optical coupling from the tipped fiber, the ferrule-top probe fabrication process needs a small modification.

4.2.2 Ferrule-top Probe Fabrication

Previously we reported methods to entirely carve the cantilever using a laser ablation system (Optec System with Lumera Laser source) [17, 18, 19]. Here we present an alternative fabrication process that minimizes the use of laser ablation and instead uses a wire cutter for bulk material removal. Some of the important steps of ferrule-top fabrication processes are shown in Fig. 4.5.

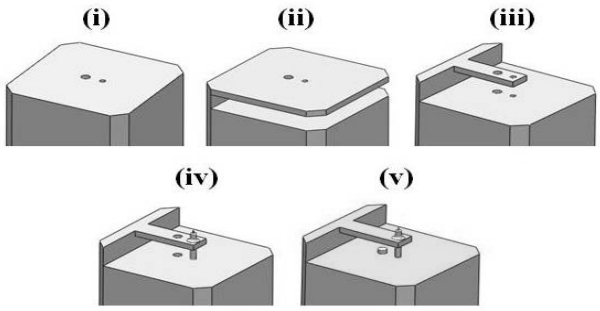

Fig 4.5 Probe fabrication process (see text for details).

The building block for a ferrule-top probe is a glass ferrule (3 X 3 X 7 mm) with two bore holes of 125 μm and 50 μm diameter [FIG. 4.5 (i)]. As a first step for fabrication, the glass ferrule is mounted on the wire cutter (Well Diamantdrahtsagen GmbH) to obtain a *flap* like structure on top of the glass ferrule [FIG. 4.5 (ii)]. The thickness of this flap determines the thickness of the cantilever. With this method of fabrication, one can obtain cantilevers with thickness of 45 μm onwards. The ferrule with *flap* is then mounted on the laser ablation system to cut the portions of the flap to obtain a cantilever of desired shape and dimensions as shown in FIG. 4.5 (iii). A tipped optical fiber [16] is then slid in to the 50 μm bore hole and fixed as shown in FIG. 4.5 (iv). The hole in the cantilever is filled with UV curable glue and the probe is then coated with Chromium (10 nm) + Gold (50 nm) in a sputtering system [FIG. 4.5 (v)]. At this point a cleaved optical fiber is slid into the 125 μm hole, which forms the detection fiber to measure the deflection of the cantilever. During the fabrication of ferrule-top cantilever probe, at the process step shown in Figure. 4.6, the tipped fiber base is ablated off to release the cantilever. Instead of ablating off the tipped fiber, a focused ion beam cut needs to be made to release the cantilever and achieve optical coupling from the tip. The focused ion beam cut ensures optically smooth surfaces for optimum light coupling, which

cannot be achieved by laser ablation. The schematic of modified ferrule-top cantilever probe with focused ion beam cut is shown in the scanning electron microscope image shown in Fig. 4.6.

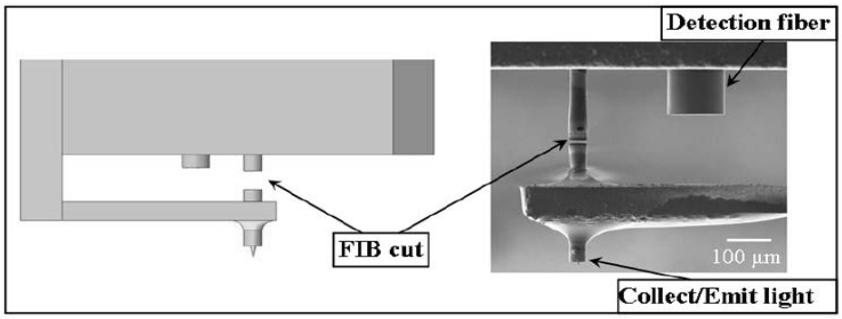

Fig. 4.6 Focused ion beam (FIB) cut to realize the cantilever and optimize optical coupling from/to the tip.

As shown in Figure. 4.6, with the FIB cut on tipped fiber, light can be coupled in or collected from the tip. The FIB cut creates sufficient gap (~3µm) to allow unrestricted bending of the cantilever and at the same time ensures adequate optical coupling. As the entire probe coated with Cr+Au during the fabrication process, FIB was used to remove this metal coating from the tip aperture to ensure light transmission through the tip. Depending upon mode of operation, i.e. light collection or emission, the tipped fiber can be connected to a photomultiplier tube (PMT) or to a laser source respectively. The detection fiber (shown in Fig. 4.6) is connected to readout to monitor the cantilever deflection while scanning.

4.2.3 Experimental Setup and Results

The schematic of the setup used for combined AFM and optical transmission microscopy is shown in Figure. 4.7.

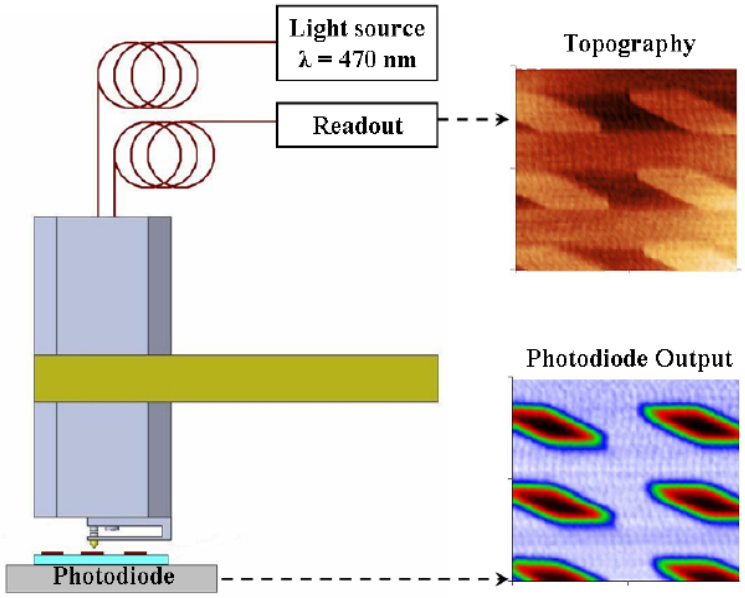

Fig. 4.7 Schematic of the setup for combined AFM and optical transmission microscopy.

To demonstrate the feasibility of combined AFM and optical transmission microscopy, the tipped fiber was connected to a laser source (λ = 470 nm). A calibration grating (SNG01, NT-MDT) with periodic rhomboidal patches of vanadium (20-30 nm) on quartz substrate was mounted on a photodiode.

The output of the photodiode after amplification was acquired as an auxiliary data channel. The probe was scanned over the grating sample in contact mode, with, the detection fiber monitoring the deflection of the cantilever and the tipped fiber illuminating the sample with 470 nm laser light. The sample topography image acquired during the scan and simultaneous optical transmission measured by the photodiode are shown in Figure 4.7. It can be seen from the two images (topography and photodiode output) that, when the tip is scanning over the vanadium metal coating, the optical transmission to photodiode is almost blocked. On the other hand, when the tip is scanning over the quartz surface, the photodiode records the highest transmission signal. At the edges of the metal coating, the tip aperture size and the distance of the grating from the photodiode surface, dominates the optical transmission. The lateral resolution of optical transmission can be improved through optimizing the ferrule-top probe fabrication process. One can achieve this by avoiding the metal deposition (Cr+Au) on tip of the fiber during the fabrication process and hence avoid use of FIB to remove the metal at the tip aperture. To further improve the optical signal quality, one can consider use of multimode optical fiber to enhance the transmission in visible wavelength range.

4.3 CONCLUSIONS

We demonstrated here capability of fiber-top and ferrule-top cantilever probe for near field detection and optical property characterization at nanoscale. These experiments show that fiber-top technology can be used for the development of a new generation of hybrid probes that can combine the double functionality of atomic force microscope and scanning near field microscopy, facilitating stand applications as well as applications in critical environments (e.g. low temperatures) both in pure collection mode (as demonstrated here) and in illumination-collection mode (where the tip is used for both illumination and light collection). At the same time ferrule-top cantilever probes also demonstrate dual functionality with cost effective fabrication approach.

REFERENCES

[1] A. Lewis, M. Isaacson, A. Harootunian, and A. Muray, Ultramicroscopy 13, 227 (1984).

[2] D.W. Pohl, W. Denk, and M. Lanz, Appl. Phys. Lett. 44, 651(1984).

[3] R.C. Dunn, Chem.Rev. 99, 2891(1999).

[4] C. Mihalcea, W. Scholz, , S. Werner, S. Münster, E. Oesterschulze, and R. Kassing, Appl. Phys. Lett. 68, 3531 (1996).

[5] C. Werner, O. Rudow, C. Mihalcea, and E. Oesterschulze, Appl. Phys. A66, S367 (1998).

[6] K. Karrai, and R.D. Grober, Appl. Phys. Lett. 66, 1842 (1995).

[7] P.N. Minh, T.Ono, H. Watanabe, S.S. Lee, Y. Haga, and M. Esashi, Appl. Phys. Lett. 79, 3020 (2001).

[8] D. Iannuzzi, S. Deladi, J. W. Berenschot, S. de Man, K. Heeck, and M. C. Elwenspoek, Rev. Sci. Instr. 77, 106105 (2006).

[9] A. Mannoni, F. Quercioli, B. Tiribilli, C. Ascoli, P. Baschieri, and C. Frediani, J. Lightwave Technol. 16, 388 (1998).

[10] S. Deladi, D. Iannuzzi, V. J. Gadgil, R. G. P. Sanders, H. Schreuders, and M. C. Elwenspoek, J. Micromech.Microeng. 16, 886 (2006)

[12] E. Betzig, J. K. Trautman, T. D. Harris, J. S. Weiner, and R. L. Kostelak, *Science* 22, 1468 (1991).

[13] P. Lambelet, A. Sayah, M. Pfeffer, C. Philipona, and F. Marquis-Weible, Appl. Opt. 37, 7289 (1998).

[14] R. Stöckle, C. Fokas, V. Deckert, R. Zenobi, B. Sick, B. Hecht, and U. P. Wild, Appl. Phys. Lett. 75, 160 (1999).

[15] N. Chevalier, Y. Sonnefraud, J. F. Motte, S. Huant, and K. Karrai, Rev. Sci. Instrum. 77, 063704-1 (2006).

[16] T. Pangaribuan, K. Yamada, S. Jiang, H. Oshawa, and M. Ohtsu, Jpn. J. Appl. Phys. 31, 1302 (1992).

[17] G. Gruca, S. de Man, M. Slaman, J. H. Rector, and D. Iannuzzi, Meas. Sci. Technol. 2, 094033 (2010).

[18] D. Chavan, G. Gruca, S. de Man, M. Slaman, J. H. Rector, K. Heeck, and D. Iannuzzi, Rev. Sci. Instrum. 81, 123702 (2010).

[19] D. Chavan, D. Andres, and D. Iannuzzi, Review of Scientific Instruments, 82, 046107 (2011).

Chapter -5

Nanoindentation – I

In previous chapters we demonstrated applicability of ferrule-top cantilever probes for nanoscale imaging and optical surface analysis. In this chapter we demonstrate that ferrule-top cantilevers can be also used to develop nanoindenters. The ferrule-top nanoindenter combines the sensitivity of commercial AFM-based indentation with the ease-of-use of more macroscopic instrumented indenters available today on the market. Furthermore, the all-optical design allows smooth operations also in liquids, where other devices are much more limited and often provide data that are difficult to interpret. This instrument may pave the way to the implementation of a new generation user-friendly nanoindenters for the measurement of the stiffness of samples in material sciences and medical research.

Adapted from: "Ferrule-top nanoindenter: an optomechanical fiber sensor for nanoindentation"
REVIEW OF SCIENTIFIC INSTRUMENTS 83, 115110 (2012)
D. Chavan, T.C. van de Watering, G. Gruca, J. H. Rector, K. Heeck, M. Slaman and D. Iannuzzi

5.1 INTRODUCTION

Material property research is one of the oldest disciplines of science and engineering, wherein the purpose of material testing was to establish appropriateness of the material for its intended use. Different material tests like hardness, scratch, wear, tensile, compression, etc. aim at understanding the material response under the conditions it will be subjected. With growing need for standardization of these material tests and quality control in manufacturing industry, macro/micro indentation tests like Brinell, Vickers, Knoop, Meyer, Rockwell, Shore and Barcol tests were proposed to test the hardness of the material. These hardness tests have their characteristic indenter geometry and hardness scales. The selection of the testing method is based on type material to be tested and thickness of the material. This hardness value of the material is usually given by the load applied divided by the area of impression upon unloading. This area of impression is usually calculated by measuring the dimensions of the impression directly or by means of optical micrograph

With further development in field of material science and its application in the field of biomedical and biophysics research, a need was realized for material characterization of more complex highly compliant materials like tissues, biomaterials, polymers etc. Hence, previously used loading parameters of macro indentations used for characterizing metals and ceramics, were not applicable for these soft materials. This gave rise to a different scale of indentation testing known as micro/nano-indentation, wherein the peak loads range from nanonewton to milenewton, indentation depths range from nanometers to micrometers and tip geometry can range from tens of nanometer to hundreds of micron. These indentation scales results in residual impressions ranging from few nanometer to hundreds of micron. This makes the estimation of area of residual impression difficult if not impossible. Furthermore the biomaterials, tissues and polymers exhibit elastic-plastic behavior and due to elastic recovery of material after unloading, the resulting impression area is much less then the area at peak load. This results in underestimation of residual impression area and

overestimation of the material stiffness. Hence, to overcome this limitation of micro/nano-indentation, a technique named *Depth Sensing Indentation* (DSI) was proposed by Oliver and Pharr [1].

In depth sensing indentation, the indenter of known geometry (sphere, cone, etc) is pressed against the sample and simultaneously the indentation (penetration) of the tip into the sample is measured. With this information about the penetration depth at the peak load and knowledge about the tip's geometrical dimensions, one can calculate the area of contact at the peak load, which can be used to calculate the hardness of the material. The characteristic load versus indentation depth curve can also provides host of information like the young's modulus, creep, plastic deformation, elastic recovery, adhesive forces, contact stiffness, frequency response, etc. of the material. As depth sensing indentation doesn't require making optical micrograph of the residual impression and is applicable to broad range of materials, is widely accepted standard for indentation testing at micro/nano-scale for compliant elastic-plastic materials. One must also understand that depth sensing indentation that provides much simplicity for micro/nano-indentation testing, doesn't provide any information about the phenomenon occurring outside the indenter-sample contact zone, namely cracks, pile-up, sink-in, which can only be observed via an optical micrograph of the residual impression.

Currently, micro/nano-indentation is performed using instrumented indenters [2] or atomic force microscope (AFM) [3]. In spite of their success, both the instruments come with some drawbacks. Most instrumented indenters are typically equipped with a stiff force sensor that limits the overall force resolution to a few microNewtons. Moreover, if the sample is submerged in a liquid medium, the force due to the water meniscus on the shaft of the indenter makes the indentation data analysis more complicated [4]. On other hand, AFMs offer better force resolution (below nanoNewtons) an advantage that has been widely used in several experiments focused on soft polymers [5,6], tissues [7,8] and cells [9,10]. Nevertheless, the use of AFMs outside research laboratories is hampered by

the complexity of the instrument. Furthermore, in order to perform AFM indentation in a liquid, one needs to mount the sample inside a specially designed fluid chamber, which limits the sample size to a few squared centimeters and increases the complexity of the apparatus even more.

In this chapter, we extend the scope of ferrule-top technology for indentation and perform indentation testing of polymer samples in air and liquid. The device has force resolution comparable to the one achieved by AFMs while maintaining the ease of use of instrumented indenters.

5.2 FERRULE-TOP NANOINDENTATION

5.2.1 Probe Fabrication

Ferrule-top cantilevers are obtained by carving a cantilever on top of a glass ferrule. Fig. 5.3 shows the most important steps of the fabrication process. The building block is a 3 mm X 3 mm X 7 mm borosilicate glass ferrule with a 50 μm and a 125 μm bore holes (Fig.5.1(i)). The glass ferrule is mounted on a ps-laser ablation system (Optec System with Lumera Laser source) to carve a central ridge and a lateral groove (Fig. 5.1(ii)) [11,12,13]. The latter is designed to host a fiber terminated with a spherical tip, which will be eventually used to indent the sample. The spherical indentation tip is obtained by melting a chemically etched optical fiber with a high current spark. The radius of the sphere can be adjusted by properly setting the etching time, and, hence, the radius of the fiber.

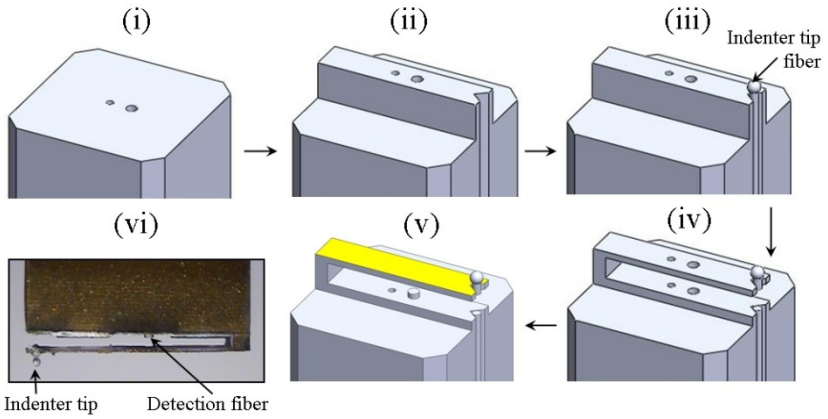

Fig. 5.1 Fabrication process for ferrule-top indenter probes (not to scale): we refer the reader to the main text for a detailed explanation of the steps illustrated.

This technique proves to be highly reproducible and to provide an optically smooth spherical tip. Alternatively, sharp conical indentation tips (radius ~ 100 nm) can be obtained by etching a special highly doped germanium fiber in buffered HF [14]. Fig. 5.2 shows the scanning electron microscope images of the tips fabricated with the methods described above. In this study, which is focused on indentation of compliant soft materials, we only use large radius spherical indentation tips (Fig. 5.2 (c) and (d)).

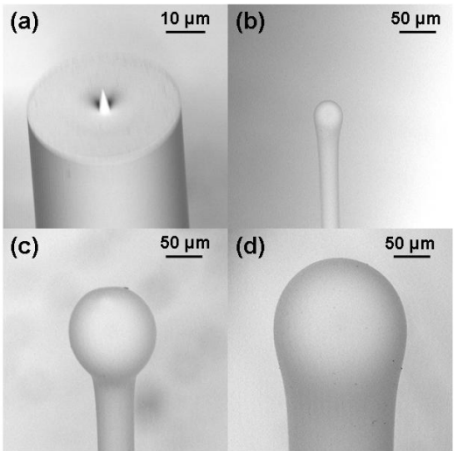

Fig. 5.2 Indentation tips of different sizes obtained by modifying optical fibers.

After the tipped fiber is glued in the groove (Fig. 5.1(iii)), the ferrule is mounted on the laser ablation system to perform the undercut and release the cantilever (Fig. 5.1(iv)). The 125 µm hole in the cantilever is filled by UV curable glue (Norland 68) followed by sputtering of chromium (10 nm) and gold (50 nm). Finally, a cleaved single mode optical fiber (Corning SMF28) is slid into the 125 µm bore hole (Fig. 5.1(v)). The other end of this fiber is connected to an optical fiber interferometer readout, which will be described later in the text. The spring constant of the cantilever largely depends on the geometrical dimensions chosen during the fabrication process. For the experiments reported in this paper, we used three ferrule-top cantilever probes, whose characteristics are reported in Table 5.1. The nominal stiffness of the cantilever was calculated from the dimensions of the cantilever.

TABLE 5.1. Ferrule-top indenter probes used for indentation experiments.

	Indenter shape	Indenter tip radius (μm)	Nominal Cantilever stiffness (N/m)
Probe – 1	Sphere	55	31
Probe – 2	Sphere	80	66
Probe – 3	Sphere	80	34

5.2.2 Nanoindenter Experimental Setup

Fig. 5.3 shows a sketch of the ferrule-top indenter developed for this experiment. The ferrule-top indenter probe is glued to a small piece of iron, which is attached to a magnet anchored to a coarse z-positioner. The sample is mounted on a closed-loop z-piezoelectric translator (P-611.ZS, PI GmbH) equipped with an integrated strain gauge sensor and controlled by a closed-loop servo controller (E-665.SR, PI GmbH). This translator is used to bring about the desired indentation stroke of up to 100 μm, with 2 nm resolution and nonlinearity of 0.1%. To give the user the possibility to indent different points of the sample, the z-piezoelectric translator is screwed on a xy-translation stage (PI GmbH). To reduce acoustic and seismic noise, the entire setup is mounted on an active vibration isolation stage (Nano-20, Accurion GmbH) housed inside an anechoic box. The setup is controlled via a Labview program that allows the user to select the desired depth and speed of the indentation stroke. The data acquired by the program during the measurement are analyzed using a separate in-house developed data analysis program.

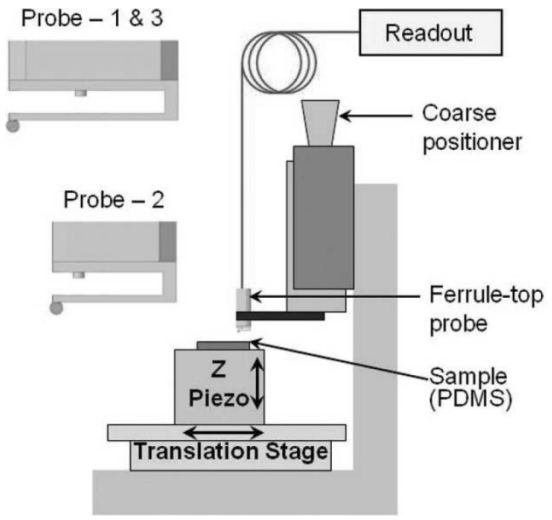

Fig. 5.3 Schematic view of the ferrule-top nanoindenter setup

5.2.3 Readout Scheme

The readout connected to the other end of the ferrule-top probe measures the deflection of the cantilever during indentation via Fabry-Pérot interferometry as explained in previous chapters (refer Pg. 27). Before the start of the indentation experiment, it is first convenient to adjust the interference signal W_0 at the midpoint of the fringe, i.e., at quadrature. Using this setting, the readout provides a linear signal both when the cantilever bends backwards during forward indention and when the cantilever, trapped by contact forces, bends forward during the retraction of the indenting tip. The midpoint can be achieved by either tuning the dimensions of the Fabry-Pérot cavity or by tuning the wavelength of the light source. Due to the limitations of the fabrication process, the only

viable solution is to tune the wavelength of the light source. The light source thus consists of a broadband superluminescent diode (SLD) (SM Benchtop SLD Source, 1550 nm central wavelength, 22 mW, 45 nm bandwidth, Thorlabs GmbH) connected to a manual fiber optic tunable filter (Agiltron Inc.), which can be tuned to reach quadrature. The schematic of this interferometer is shown in Fig. 5.4.

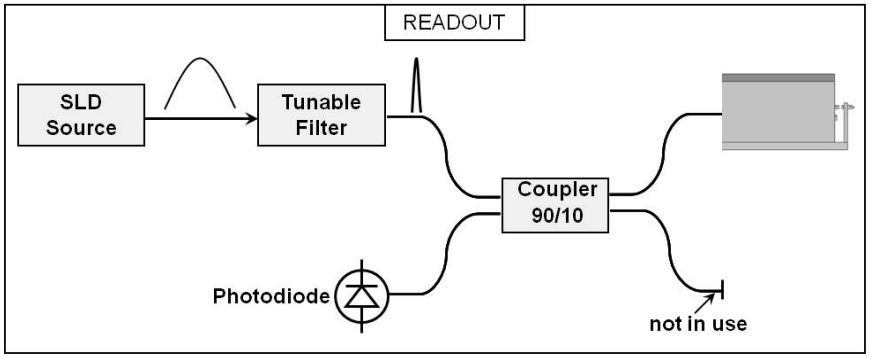

Fig. 5.4 Readout with tunable filter for ferrule-top cantilever probe.

The output of the fiber optic tunable filter is connected to a 90/10 coupler. The 10% arm of the coupler is connected to the ferrule-top probe and the 90% arm is not in use. A photodiode (Newport Inc.) aligned with the forth port of the coupler is then used to measure the intensity of the light reflected back from the probe head, which is the result of the interference between the light reflected at fiber-to-gap interface, the light reflected by gap-to-cantilever interface, and the light reflected at the cantilever-to-metal interface. The advantages of this configuration are shown in Fig. 5.5, where we report the interference fringe due to bending of the cantilever upon indenting a glass as recorded with two different wavelengths: one corresponding to the midpoint (λ_1) and another one corresponding to an interference point close to a maximum of interference (λ_2).

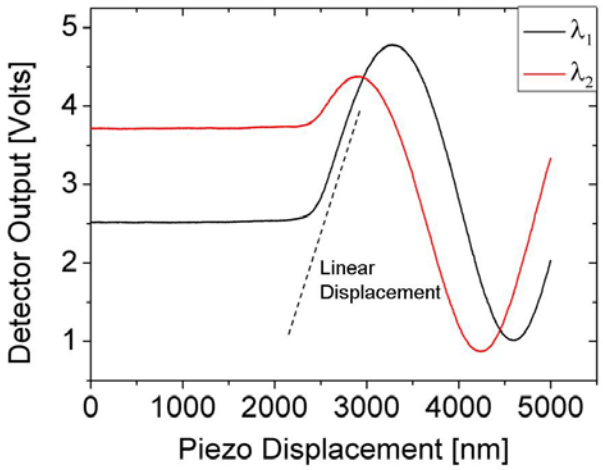

Fig. 5.5 Readout signal observed while indenting a glass sample with a ferrule-top indenter. The two lines correspond to two different wavelengths of the light source mounted in the readout. The graph is meant to illustrate the advantages (in terms of signal linearity) of working close to quadrature (λ_1) rather than close to a maximum of interference (λ_2).

To translate the detector output (in volts) to deflection of cantilever d_c (in nanometers), one needs to measure the deflection sensitivity (nm/V). This proportionality constant can be readily measured by indenting a very stiff sample (e.g. a piece of glass), so stiff that the indentation depth can be safely set to zero. Under this assumption, the indenter tip deflects the same amount as the close-loop piezo movement. From the slope of the linear part of the fringe (shown in Fig. 5.5 by the dashed line), one can thus extract the deflection sensitivity of that probe for the given laser power and detector gain. It is clear that the value obtained via this calibration measurement is only viable to analyze data in the linear part of the interference fringe, which corresponds to about one forth of λ (~387 nm). This value is sufficiently large in most indentation experiments. The deflection sensitivity for Probe

1, 2 and 3 was calculated to be 327 nm/volt, 99 nm/volt and 465 nm/volt in air respectively and 478 nm/volt for Probe 1 in water.

It is worthwhile to note that, the deflection sensitivity of a probe expressed in nm/volts varies for each probe depending upon the Fabry-Perot cavity gap length i.e. distance between the cantilever and the detection fiber, which is adjusted manually while fabricating the probe. Furthermore, the deflection sensitivity also depends on the laser power and detector gain settings, chosen to attain best possible deflection sensitivity. This explains for the variation observed in deflection sensitivity reported for Probe-1 (327nm/volt) and Probe-3 (465nm/volt). Apart from these factors, the deflection sensitivity can strongly vary with position of the detection fiber with respect to the indentation tip. For Probe-1 and Probe-3 the detection fiber is in the middle of the cantilever (~1.5 mm away from the indentation tip), identical to the one shown in fabrication process (Fig.5.3). For Probe-2, the detection fiber is close to the indentation tip (~ 250 μm away from the indentation tip), identical to the probe configuration shown in Fig. 5.5. The Probe-2 configuration is adopted to have shorter and more stiffer cantilevers (66 N/m). Additionally, the deflection sensitivity of Probe-1 in liquid (478 nm/volt) varies from deflection sensitivity from air due to change in refractive index of the medium, laser power and detector gain settings adopted during the experiment.

The force resolution of our setup is determined by the random fluctuations of the length of the Fabry-Perot cavity formed between the detection fiber and the cantilever, which are induced by the coupling of acoustic and mechanical vibrations into the probe. Those fluctuations produce the dominant part of the noise at the output of the readout (expressed in Volts) that, multiplied by the deflection sensitivity (expressed in m/V) and by the spring constant of the cantilever (expressed in N/m), provides the force noise. For our setup, in air the rms noise at the output of the readout, sampled at a 1000 sample/s, is approximately 2 mV. For a typical ferrule-top probe (deflection sensitivity ~ 300 nm/V) results in cantilever deflection resolution of 6Å, hence for cantilever with spring constant ~ 30 N/m, the force sensitivity of a probe corresponds to 18 nN.

5.2.4 Experimental Procedure And Working Principle

Indentation was performed on PDMS (polydimethylsiloxane, Sylgard-184, Dow Corning, Inc) samples of two different moduli, obtained by mixing the elastomer and the cross linking agent in ratios of 10:1 and 20:1, respectively. The two mixtures (10:1 and 20:1) were allowed to degas for 30 min to remove air bubbles, and kept in a oven at 100°C for 45 min to cure the PDMS before use. The thickness of the samples was in the order of 2 to 3 mm. Sample pieces of size 10 mm X 10 mm were cut and glued to a petri dish, which was mounted on top of the z-piezoelectric translator. Indentation curves were obtained with the following procedure. The probe was first brought close to the sample (PDMS) by the coarse positioner within a separation distance of few tens of microns. The sample was then moved by the z-piezoelectric translator at a rate of 1 μm/s towards the probe until, after entering in contact with the indentation tip of the ferrule-top probe, it would have induced the cantilever to bend backwards for a few tens of nanometers. At the end of this procedure, the z-piezoelectric translator retracted the sample a few microns away from the indenting tip. This position was set as the initial vertical point of all the following indentation curves. Starting from this position, several different points of the sample (selected via the xy translational stage) were finally indented with a loading and unloading rate of 1 μm/s.

To test the ferrule-top indenter in liquids, we simply filled the petri dish with water. The probe was then lowered into the petri dish with the coarse positioner, and the indentation procedure was repeated following the same procedure as for the indentation in air, including the measurement of the deflection sensitivity at the start of the measurements.

From these indentation tests, the indentation depth (d_i) can be obtained by subtracting the deflection of the cantilever measured by the interferometer (d_c) to the piezo displacement (d_p):

$$d_i = d_p - d_c \tag{5.1}$$

The load applied during the indentation cycle is given by:

$$P = k \cdot d_c \tag{5.2}$$

where k is the stiffness of the cantilever as listed in Table 5.1.

The raw indentation data acquired from the indentation program were further processed to estimate the Young's modulus following an algorithm that is explained in the next section. For the measurements in air, at least 15 indentation curves, obtained in different points of the sample, were considered for each probe (1, 2 and 3) and for each sample (10:1 and 20:1). Indentation in liquid was performed only with probe I, with 9 indentation curves for the 10:1 sample and with 8 curves for the 20:1 sample. The indentation spots were at least 0.5 mm apart from each other.

5.3 RESULTS AND DISCUSSION

Hertzian contact mechanics [16] is a classical theory that can be used to quantitatively estimate the material properties of an elastic sample from indentation data. Following this theory, one can write the load P applied by the indenter in terms of the reduced Young moduli of the indenting material E_1 and of the indented material E_2:

$$P = \frac{4}{3} E^* R^{\frac{1}{2}} d_i^{\frac{3}{2}} \tag{5.3}$$

where R is the indenter tip radius, d_i is the indentation depth, and E^* is the reduced modulus, which is given by:

$$\frac{1}{E^*} = \frac{1-\nu_1^2}{E_1} + \frac{1-\nu_2^2}{E_2} \tag{5.4}$$

where ν_1 and ν_2 are the Poisson's ratios of the indenting and of the indented materials, respectively. Hertz model applies only to fully elastic contacts with small indentation depths (as compared to the indenter radius) and no adhesive forces. However, during indentation of compliant materials, adhesive and capillary forces between the tip and the sample cannot be neglected. To take into account this effect, it is more appropriate to use either the Johnson-Kendall-Roberts (JKR) [17] or the Derjaguin-Muller-Toporov (DMT) [18] model. The JKR model predicts the indentation behavior of a soft material by a large indenter tip radius, whereas the DMT model predicts the indentation behavior of a stiffer material with a smaller indenter tip radius. To determine which of the two models is more appropriate, one can calculate the Tabor coefficient [19], which is given by:

$$\mu = \left(\frac{R \cdot \Delta\gamma^2}{E^{*2} z_0^3} \right)^{\frac{1}{3}} \tag{5.5}$$

where R is the indentation tip radius, $\Delta\gamma$ is the work of adhesion, E^* is the reduced sample modulus and z_0 is the equilibrium separation between atoms. The DMT and JKR model can be safely applied for $\mu < 0.1$ and $\mu > 5$. For $0.1 < \mu < 5$ other models have been developed [20].

In order to assess the value of the Tabor coefficient for our experimental conditions, we first need to estimate the value of $\Delta\gamma$. Fig. 5.6 shows a typical load-versus-indentation curve obtained while indenting with Probe 1 the 10:1 PDMS sample.

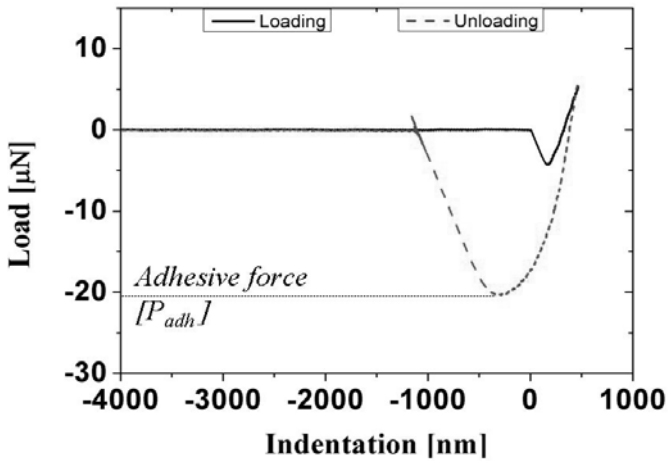

Fig. 5.6 Load versus indentation depth curves obtained while indenting the PDMS 10:1 sample with Probe 1.

The role of adhesive forces is quite evident, as it causes a deep minimum in the unloading curve. This minimum can be used to roughly estimate the work of adhesion according to:

$$\Delta\gamma = -\frac{2}{3}\frac{P_{adh}}{\pi R} \tag{5.6}$$

where P_{adh} can be taken as the value of the minimum in the unloading curve. For P_{adh} ≈20 μN, R=55 μm, E ≈5 MPa and z_0≈0.5 nm [21], one obtains μ≈470 (>>5) which indicates that, for the analysis of this set of data, the JKR model is more appropriate. Similar results can be retrieved for all the other in-air experiments.

To simplify the analysis of the experimental curves, we have followed the JKR 2-Point method [21, 22], which makes use of only two points of the unloading curve (see Fig. 5.7).

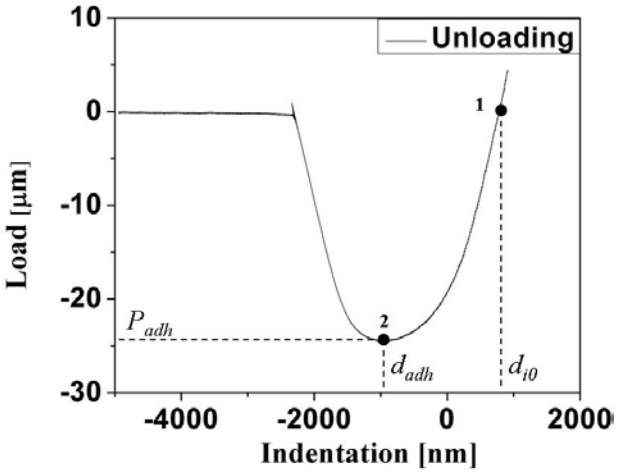

Fig. 5.7 Illustration of the 2-Point analysis method.

The first point (point 1 of Fig. 5.7) corresponds to the point where the unloading curve crosses the zero load line. This point gives the indentation depth for zero load (d_{i0}). The second point (point 2 of Fig. 5.7) corresponds to the maximum adhesion point of unloading curve, which gives the negative adhesive load (P_{adh}) and the negative indentation depth (d_{iadh}). The

values d_{i0}, d_{iadh} and P_{adh} obtained from the unloading part for each indentation curve, can be then used to calculate the sample modulus according to [21]:

$$E^* = -\frac{3P_{adh}}{\sqrt{R}}\left[\frac{3(d_{i0}-d_{iadh})}{1+4^{-2/3}}\right]^{-3/2} \tag{5.7}$$

Table 5.2 shows the Young modulus of the two PDMS samples (10:1 and 20:1) as measured with the three probes. The modulus values measured by all the three probes are in good agreement with those published in the literature [23, 24]. It is still important to stress that, by using the nominal value of the spring constant of the cantilever to convert cantilever bending into force, we may have introduced a significant systematic error.

TABLE 5.2. Result of the measurement of the reduced Young modulus of two PDMS samples with three different probes.

	PDMS (MPa) 10:1	PDMS (MPa) 20:1	Modulus Ratio 10:1/20:1
Probe – 1	4.60 ± 0.12	1.43 ± 0.11	3.21
Probe – 2	3.41 ± 0.20	1.10 ± 0.04	3.10
Probe – 3	4.49 ± 0.10	1.44 ± 0.07	3.12

The validity of our method can then be checked by looking at the ratio between the Young modulus measured for the 10:1 sample and that measured for the 20:1 sample. This parameter gives the relative stiffness

between the two samples, and is thus not affected by the systematic error discussed above. The modulus ratios measured by the three probes, also reported in Table 5.2, show indeed good consistency between different experiments.

In Fig. 5.8 we report a representative load-versus-indentation curve obtained while indenting, with Probe 1, the 20:1 sample immersed in water. It is evident that the presence of water reduces adhesion and capillary effects to negligible levels. Because of the absence of adhesive forces and residual impression, data obtained in water can be elaborated via the Hertz model (Eq.(5.3)). Following this procedure, we obtained a Young modulus of 2.28 ± 0.23 MPa and 0.95 ± 0.21 MPa for the 10:1 and 20:1 sample, respectively, with a modulus ratio of 2.40 (as measured with Probe 1; Probe 2 and Probe 3 were not used in water). The periodic noise pattern observed for indentation curves in liquid (see Fig. 5.8), has contribution from frequencies in range of 32 – 52 Hz. We suspect this low frequency noise can arise from the mechanical vibrations sensed by the Fabry-Perot cavity.

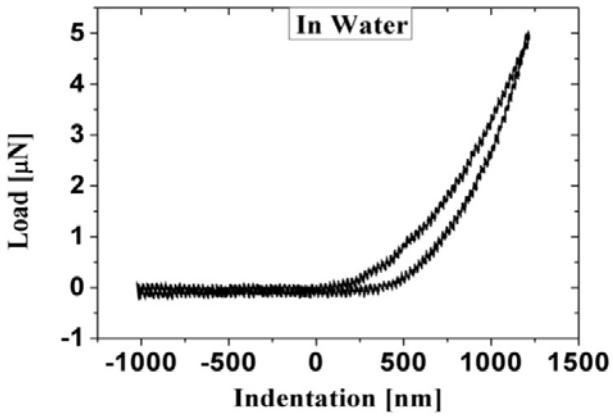

Fig. 5.8 Load versus indentation depth for indentation of PDMS (20:1) in liquid by Probe 1.

The sample moduli and the modulus ratio calculated for indentations performed in liquid deviates appreciably from those measured for the same sample in air. Similar deviation in modulus values of PDMS measured in air and aqueous solution are reported earlier [24]. The origin of this effect is still not completely understood. Other factors that can influence the calculated sample modulus in air and water are surface roughness, surface contaminations, thermal drifts, deviation from actual tip geometry, variation in deflection sensitivity of the cantilever due to laser power variation, and nonlinearities of the piezo. These kinds of problems are common to other techniques, and their analysis goes beyond the scope of present research goal. This work should in fact not be taken as an attempt to provide a metrological assessment of the mechanical properties of PDMS but more as a demonstration of device capability for indentation in air and liquids.

Concerning the overall force resolution, it is important to stress that, because of mechanical vibrations, when the probe is in contact with the sample the noise at the output of the readout is generally different with respect to that measured before contact. To quantify this effect, we have fit the indentation data with a spline curve and analyzed the residuals with standard statistical algorithm. According to this analysis, the force noise of Probe-1 during indentation of PDMS 20:1, for example, is equal to ~40 nN and ~60 nN in air and in water, respectively. The force noise observed in water is slightly higher because of the effect of the capillary bridge on the side of the probe holder. This force noise can further vary for different probes and the material indented.

5.4 CONCLUSIONS

We have presented a novel device for material property characterization. The instrument is easy to use both in air and water, and can accommodate samples of any size. The sample moduli estimated by the device when tested on a polymer sample are consistent and in good agreement with the values reported in the literature. We envision applications for *in situ* experiments

and integration into other scientific instruments. Because the indenter tip is part of an optical fiber, it is feasible to develop devices where one can indent a sample while also coupling light from or to the indentation point. This opens new possibilities for simultaneous mechanical and optical characterization of materials.

REFERENCES

[1] W. C. Oliver, and G. M. Pharr, Journal of Materials Research, 7, 1564 (1992).

[2] M. R. VanLandingham, Journal of Research of the National Institute of Standards and Technology, 108, 249 (2003).

[3] G. Binnig, C. F. Quate, and Ch. Gerber, Phys. Rev. Lett. 56, 930 (1986).

[4] A. B. Mann, and J. B. Pethica, Langmuir, 12, 4583 (1996).

[5] M. R. VanLandingham, J. S. Villarrubia, W. F. Guthrie, and G. F. Meyers, Macromolecular Symposia, 167, 15 (2001).

[6] G. Moeller, and V. Domnich, Microscopy and Microanalysis, 13, 186 (2007).

[7] S. Hengsberger, A. Kulik, and Ph. Zysset, European Cell and Materials, 1, 12 (2001).

[8] Y. X. Zhu, Z. X. Dong, U. C. Wejinya, S. Jin, and K. M. Ye, Journal of Biomechanics, 44, 2356 (2011).

[9] S. E. Cross, Y. S. Jin, J. Rao, and J. K. Gimzewski, Nature Nanotechnology, 2, 780 (2007).

[10] Q. S. Li, G. Y. H. Lee, C. N. Ong, and C. T. Lim, Biochemical and Biophysical Research Communications, 374, 609 (2008).

[11] G. Gruca, S. de Man, M. Slaman, J. H. Rector, and D. Iannuzzi, Proc. SPIE 7503, PDP07 (2010).

[12] D. Chavan, G. Gruca, S. de Man, M. Slaman, J. H. Rector, K. Heeck, and D. Iannuzzi, Review of Scientific Instruments, 81, 123702 (2010).

[13] D. Chavan, D. Andres, and D. Iannuzzi, Review of Scientific Instruments, 82, 046107 (2011).

[14] T. Pangaribuan, K. Yamada, S. Jiang, H. Oshawa, and M. Ohtsu, Jpn. J. Appl. Phys. 31, 1302 (1992).

[15] D. Iannuzzi, S. Deladi, V. J. Gadgil, G. P. Sanders, H. Schreuders, and M. C. Elwenspoek, Appl. Phys. Lett. 88, 053501 (2006).

[16] H. Hertz, Miscellaneous Papers (Macmillan, London, 1896).

[17] K. L. Johnson, K. Kendall, and A. D. Roberts, Proceedings of the Royal Society of London Series a-Mathematical and Physical Sciences, 324, 301(1971).

[18] B. V. Derjaguin, V. M. Muller, and Y. P. Toporov, J. Colloid Interface Sci., 53, 314 (1975).

[19] D. Tabor, J. Colloid Interface Sci., 58, 2 (1977).

[20] D. Maugis, J. Colloid Interface Sci., 150, 243 (1992).

[21] D. M. Ebenstein, and K. J. Wahl, J. Colloid Interface Sci., 298, 652 (2006).

[22] J. C. Grunlan, X.Y. Xia, D. Rowenhorst, and W.W. Gerberich, Rev. Sci. Instrum. 72, 2804 (2001).

[23] D. M. Ebenstein, J. Mater. Res. 26, 1026 (2011).

[24] F. Carrillo, S. Gupta, M. Balooch, S. J. Marshall, G. W. Marshall, L. Pruitt and C. M. Puttlitz, J. Mater. Sci. 20, 2820 (2005).

Chapter 6

Nanoindentation - II

In previous chapters we demonstrated use of ferrule-top cantilever probe for AFM indentation to measure the mechanical properties of polymers and biomaterials. However, such AFM indentation lacks ability to distinguish between the contributions of different layers of the sample. Here we present a further development to the ferrule-top probe that combines optical coherence elastography (OCE) depth sensing with AFM indentation. The new probe hosts underneath the cantilever two optical fibers. One of them is coupled to an interferometer that can remotely measure the bending of the cantilever with nanometer precision. The other fiber, aligned with the free hanging end of the cantilever, serves as the OCT probe. The instrument brings the tip of the cantilever in contact with the sample, indents the sample with a calibrated stroke, and simultaneously assesses, via OCT, the degree of deformation induced by the stroke in each different layer of the sample.

Adapted from: "Collecting optical coherence elastography depth profiles with a micromachined cantilever probe"
OPTICS LETTERS, (2013)
D. Chavan, J. Mo, M. de Groot, A. Meijering, J. F. de Boer, and D. Iannuzzi

6.1 INTRODUCTION

Over the last few years, optical coherence elastography (OCE) [1] and atomic force microscope (AFM) indentation [2] have generated increasing interest in the broad field of material analysis. Although these two techniques are based on a similar approach, the information they provide is largely complementary. OCE relies on the use of optical coherence tomography (OCT) to look at how different subsurface layers deform when the sample is loaded with a force distributed over a macroscopic area (>1 mm^2) [3, 4]. Those data are then used to infer the mechanical response of each individual layer down to a depth of a few millimeters. In AFM indentation, a micrometer size sphere mounted on the free hanging end of a micromachined cantilever indents the sample with a force that may be as small as a few piconewtons, i.e., up to eleven orders of magnitudes smaller than the smallest force ever used in OCE. Measuring the deflection of the cantilever throughout the whole duration of the indentation stroke, one can then obtain the Young's modulus of the sample at scales that could hardly be accessed by OCE. On the other hand, AFMs lack the optical imaging capability of OCE, and can only provide data on the mechanical response of the sample as a whole, without the possibility to distinctively observe subsurface features that the external load may induce. It is thus evident that, in material analysis, one is often forced to neglect one important piece of information by choosing between either macroscopic indentation with depth sensitivity or microscopic indentation with no depth sensitivity. On the other hand, the analysis of the deformation of subsurface layer in response to an AFM-like stroke may provide information that is not accessible when the two techniques are used separately. A smaller indentation area would allow one to distinguish the mechanical contribution arising from the microscopic components of the sample, whose effect are averaged when larger contact areas are used.

Here, we present a novel device that can combines the possibility of AFM like indentation stroke to access the material surface properties and simultaneously monitors sub-surface layer deformations at the point of

indentation. This new device based on ferrule-top technology we call it *OptoMechanical NanoElastography* (OMNE) probe.

6.2 OMNE: PROBE FABRICATION

The building block of our OptoMechanical NanoElastography (OMNE) probe is a 3 mm x 3 mm x 7 mm single bore borosilicate ferrule, which is machined in the form of a 2.7 mm long, 500 μm wide, 150 μm thick cantilever (see Fig. 6.1 for the details of the fabrication process; see also [5, 6] for our previous work on ferrule-top cantilevers and ferrule-top indentation). The free hanging end of the cantilever is equipped with a tubular tip (outer diameter = 250 μm, inner diameter = 150 μm). Underneath the cantilever, the ferrule hosts two single mode optical fibers (cladding diameter = 125 μm, core diameter = 9 μm), one mounted at the center, the other aligned with the tubular tip. Light coupled from the opposite end into the central fiber is reflected by the fiber facet in front of the cantilever and by the cantilever itself. The reflected beams propagate back into the fiber, forming an interference signal whose amplitude depends on the separation between the fiber facet and the cantilever. Measuring the amplitude of the back propagating signal, one can thus infer the deflection of the cantilever, as in standard Fabry-Perot interferometers (for details, see [5]). To make sure that the output signal of the interferometer scales linearly with the deflection of the cantilever, the wavelength of the light source can be tuned to quadrature. The optical fiber aligned with the tubular tip is connected to an optical coherence tomography (OCT) readout [7, 8]. It is worthwhile to mention that the OCT optical fiber used is cleaved at ~8 degree angle to avoid high back reflection from the cleaved surface and hence saturation of the detector photodiode.

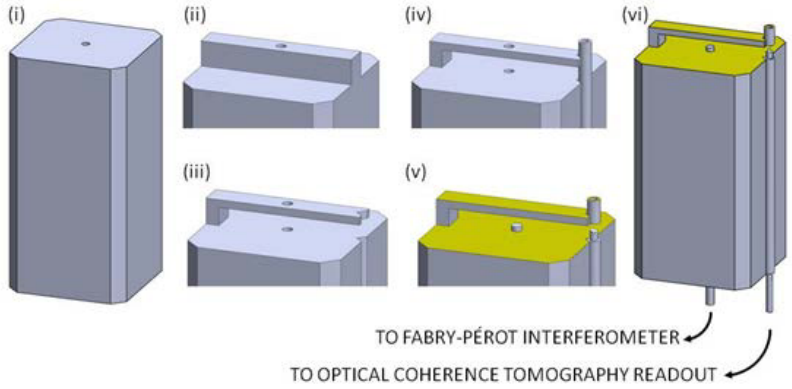

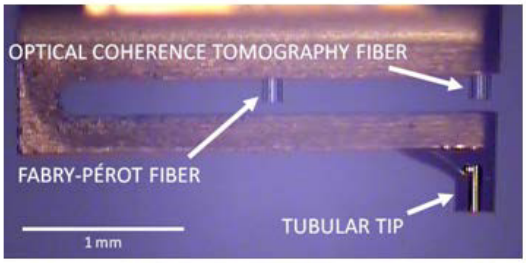

Fig. 6.1 (top) Overview of the fabrication process of the OptoMechanical NanoElastography (OMNE) ferrule-top probe used in this study. (i) The building block is a single bore borosilicate ferrule. (ii) The block is carved in the form of a rectangular ridge with a wire cutter. (iii) A v-groove is then carved on the side of the ferrule with a wire cutter, which is also used to further machine a cantilever out of the ridge. (iv) A capillary tube is laid on the v-groove and glued. (v) The tube is cut to free the cantilever; two optical fibers are then inserted into the bore hole and into the capillary tube, respectively, and glued. Finally, the top surface of the device is coated with gold. (vi) Schematics of an OMNE probe. (bottom) Microscope image of the OMNE ferrule top probe used in this study.

It is important to note that the thickness of the cantilever has been deliberately chosen to be much larger than typical to make sure that the spring constant (which, following Euler-Bernoulli beam theory, is calculated to be ≈1.5 kN/m) is sufficiently high to induce significant deformation in the subsurface layers of the samples investigated. Should the experimental conditions require, it is certainly possible to reduce the cantilever thickness to approximately 20 μm, with a decrease of the spring constant by a factor 400. An even smaller spring constant value can be achieved by cutting the cantilever along the diagonal, using larger ferrules, machining cantilevers with non-uniform width, or replacing the cantilever with other spring designs.

6.3 EXPERIMENTAL DETAILS

6.3.1 Experimental setup

The optomechanical indentation probe is anchored to a coarse manipulator to bring the indentation tip in contact with the sample to be tested. The sample is mounted on a closed-loop z-piezoelectric translator (P-611.ZS, PI GmbH) equipped with an integrated strain gauge sensor and controlled by a close-loop servo controller (E-665.SR PI GmbH). This z-piezoelectric translator brings about the required indentation stroke of up to 100 μm with 2nm resolution. The Fig. 6.2, shows the schematic of the experimental setup used and OCT readout.

The Fabry-Pérot readout (OP1550, Optics11 B.V.) is connected to the central optical fiber that monitors the deflection of the cantilever. For details about the readout we refer readers to [5, 6]. The other optical fiber aligned to the hollow capillary (indentation tip) is connected to a OCT readout [7, 8] that uses 1258 – 1366 nm, 50 kHz frequency (Axsun Technologies Inc. MA, USA) swept source to provide 50,000 depth profiles (A-lines) per second.

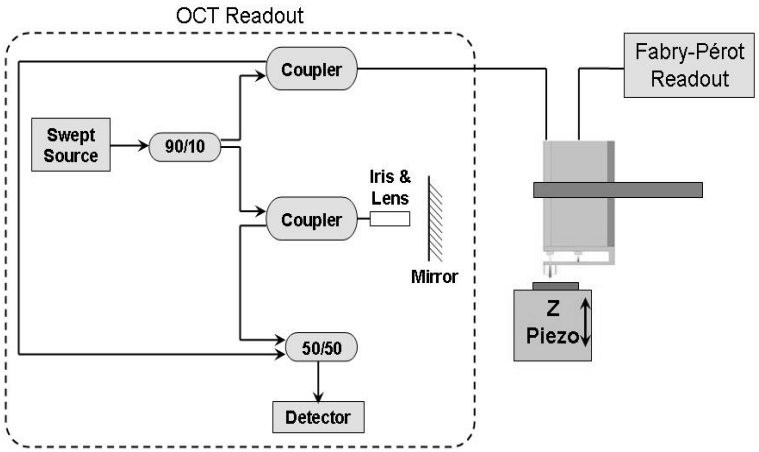

Fig. 6.2 Schematic of the experimental setup.

A Labview program is used to control the setup, which allows the user to define the indentation depth and speed of indentation. The data acquired (indentation & OCT depth profiles) during the measurement are analyzed separately. For OCT depth profile data processing, the phase of the reflection peak corresponding to the cleaved end of the optical fiber is used as a stable local phase reference and allows one to generate a continuous deformation profile for each surface via phase unwrapping [9]. The phase for each surface is calculated by an intensity-weighted average within a 5-point window around the peak in the depth profile. To decrease the noise, the calculation is performed on 10,000 lines per second, obtained by averaging the A-lines of each single run over a time window of 0.1 ms. To reduce the amount of data further, we consider only one out of every 100 points.

6.3.2 Sample Preparation

To perform indentation and simultaneously demonstrate monitoring of sublayer deformation, we chose to fabricate samples with distinct layers which can be monitored with OCT depth profiles. The first sample was prepared by stacking 3 layers of 10 X 10 X 1 mm PDMS (Sylgard 184; 30:1 elastomer to curing agent ratio). A thin layer of gold (~20nm) was sputtered on top surface of 2nd and 3rd layer to enhance the OCT signal. The second sample consists of a rectangular channel, 1mm thick and 2.4 mm wide, embedded inside a PDMS (20:1) block, at ~700 μm from the top surface. The schematic of two samples and their depth profiles as obtained by OCT readout are shown in Figure. 6.3.

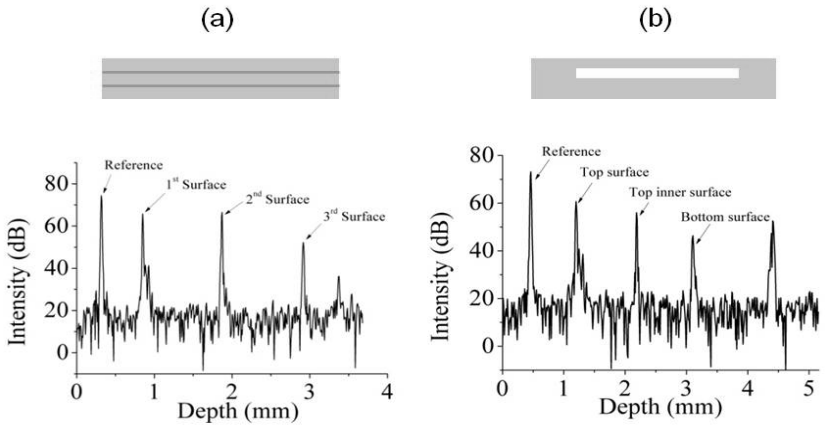

Fig. 6.3 Samples used for experiments and their respective depth profile as acquired by OCT readout (just before indentation): (a) Stack of PDMS sheets of size 10 X 10 X 1 mm (b) rectangle channel (without water) embedded within a PDMS block.

6.3.3 Experimental Procedure

Before one can start the actual indentation measurement, it is convenient to adjust the Fabry-Pérot readout output at the quadrature of the interference fringe. This way, the readout provides linear signal when the cantilever bends backwards during the indentation. This is achieved by pressing the cantilever against a very hard surface (e.g. glass slide), and changing the wavelength of the interferometer iteratively till the desired interference position is obtained. Furthermore the interference output obtained while indenting the glass slide is used to calculate the deflection sensitivity (nm/volts), to translate the cantilever deflection in volts to nanometer. For detail explanation of this procedure, we refer readers to [ref. 6].

6.4 RESULTS AND DISCUSSION

The first sample (layered PDMS) was pushed by the piezoelectric stage against the tubular tip with a 20 μm indentation stroke (approximately 10 μm pre-contact + 10 μm in-contact) at rate of 1 μm/s. As shown in Fig. 6.4, the top graph (black line) shows the deflection of the cantilever δ_C recorded, at a rate of 1000 samples/s, by the FP interferometer as a function of the elongation of the piezoelectric stage d_{pz}. The bottom graph (colored lines) shows the deformation of the outermost surface, 2nd and 3rd surfaces of the layered PDMS, simultaneously recorded with the OCT readout (δ_1, δ_2, and δ_3, respectively). As seen, the cantilever bends upwards, reaching a deflection of ~90 nm at the end of the stroke. The top surface of the sample is pushed downwards by the tubular tip over the whole perimeter of the hollow cylinder. As a reaction, the parts of the sample surface that lie within the open area of the tip slightly moves upwards inside the tube. Overall, the ~4.5 μm deep deformation of the top surface measured by our instrument in response to the maximum load is given by the difference between the two phenomena, with the first one prevailing on the second. This indentation stroke also produces a deformation of the 2nd layer of ~1 um. The load is

however not sufficient to reach the 3rd layer, which remains in the same position for the whole duration of the stroke. The measured variance of the noise for the Fabry-Perot and OCT readout corresponded to less than 2 and 15 nm, respectively.

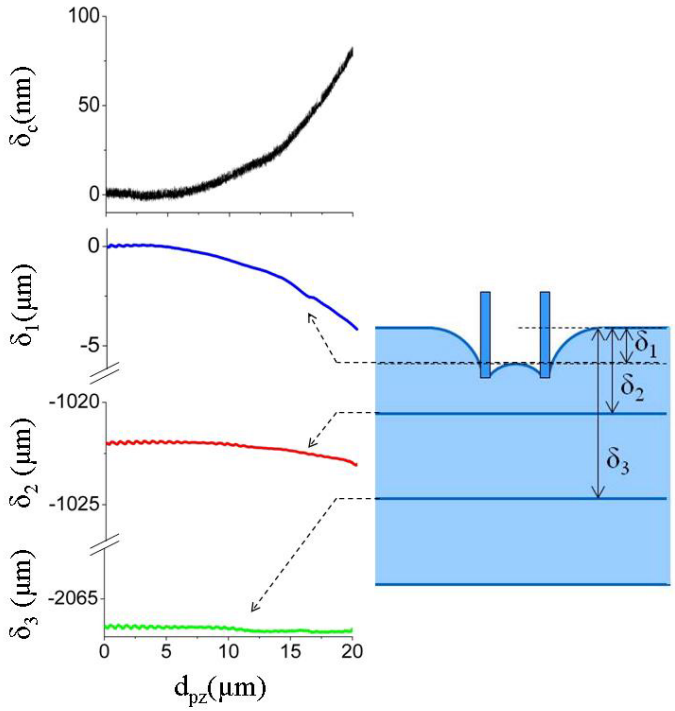

Fig. 6.4 Upper graph (black line): deflection of the cantilever as a function of the elongation of the piezoelectric stage that moves a multilayered sample against the tip of the cantilever. Bottom graph (colored lines): vertical position of the different parts of the sample during the indentation stroke as obtained from the OCT depth profile data.

The second sample (subsurface rectangular channel) was then used to demonstrate that our probe can measure the change of the stiffness in a subsurface structure. To achieve this goal, the sample was pushed by the piezoelectric stage against the tubular tip with a 30 μm long, 1 μm/s rate indentation stroke under two conditions: air-filled (channel ends not sealed) and water-filled channel (channel ends sealed). The data were then used to compare the deformation of the channel observed in the two cases. The results of this test are reported in Fig. 6.5, where we plot the thinning of the channel (as measured by the OCT readout) versus the load applied (as calculated by multiplying the deflection of the cantilever extracted from the FP signal by the nominal spring constant of the cantilever), assuming refractive indexes of PDMS and water equal to 1.4 and 1.33, respectively. The graph clearly demonstrates that our probe can measure the change of the mechanical behavior of subsurface layers.

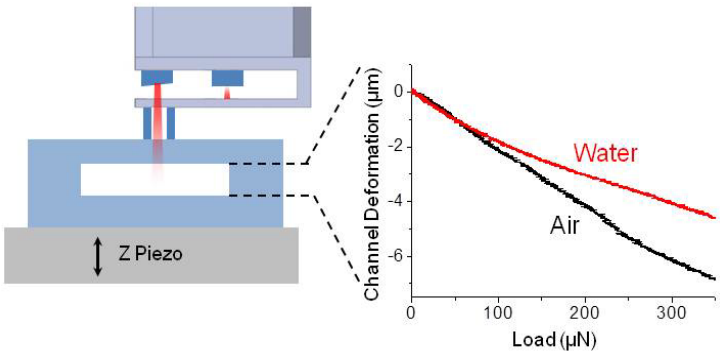

Fig. 6.5 Deformation of channel when filled with water or air.

As seen in the graph above, the channel when filled with water undergoes less deformation as compared to the channel with air, for the equal amount of applied load. The load here is calculated by multiplying cantilever displacement in nanometers with cantilever stiffness ~1.5 kN/m.

The probe used in the above experiments has a tubular indentation tip with an outer diameter of 250 μm. Thus the indenter tip dimension puts limitation on the lateral resolution for the loading area during the indentation test. Also worthwhile to remind, that the lateral resolution of the OCT depth profiles are determined by the beam size and shape.

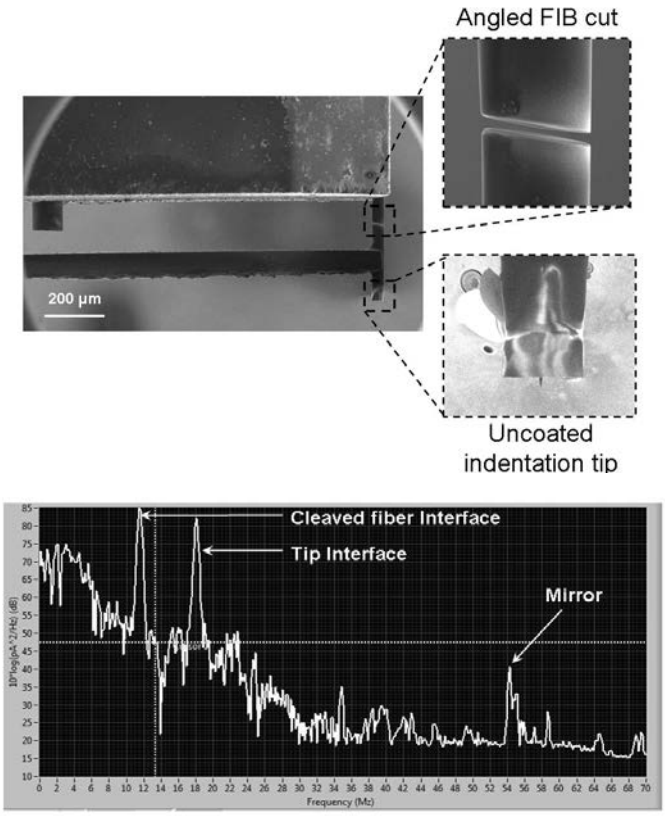

Fig. 6.6 (Top) OMNE probe with sharp indentation tip with ~8 degree angled FIB undercut. (Bottom) OCT depth profile acquired with probe mounted above the mirror.

To improve on the indentation lateral resolution, we fabricated a probe that has an indenter tip of only few hundred nanometers. The fabrication of this probe is similar to the fabrication method used to fabricate ferrule-top cantilever probe for combined AFM and optical signal collection [10]. The fabricated probe and the depth profile, acquired with the OCT system, is shown in Fig. 6.6. For this probe, the tipped fiber is connected to the OCT readout that provides the depth profile of the sample. An important change to the fabrication process was to make the focused ion beam (FIB) cut at an approximate angle of 8 degrees. The angled FIB cut is used for the same reason as the angled cleaved fiber explained previously. Unfortunately, this probe cannot be used for indentation of PDMS sample due to high stiffness of the cantilever. To use a probe with such a sharp indenting radius, one needs to fabricate cantilevers with stiffness at least one order of magnitude lower than the probe presented here.

6.5 CONCLUSIONS

We have introduced a new optomechanical micromachined probe that allows one to compress a sample with an AFM-like indentation stroke and simultaneously observe how the subsurface layers underneath the tip deform under that external load. Because of its monolithic all-optical design, the probe is easy to use and, in principle, can operate in harsh environments. The geometry of the spring and of the indenting tip can be varied to permit utilization in very different context. The indentation depth and stroke parameters can be adapted to the measurement conditions as well. A mechatronics configuration where the probe is anchored to a three-axis piezoelectric scanner that allows sequential indentation over a selected area of the sample is also feasible. This would provide a three-dimensional nanoelastography map of that area. It is fair however, to acknowledge that such a solution would still have a limited lateral resolution in the OCT depth profile as this is determined by the beam size.

We believe that this study paves the way for the development of a new generation of instruments for material analysis, with potential applications,

among others, in the medical field, where it could be used to assess the elasticity of tissues and cells down to intracellular components in pre-clinical research and clinical practice.

REFERENCES

[1] J. Schmitt, Opt. Express 3, 199 (1998).

[2] H. J. Butt, B. Cappella, and M. Kappl, Surf. Sci. Rep. 59, 1- 152 (2005).

[3] B. F. Kennedy, X. Liang, S. G. Adie, D. K. Gerstmann, B. C. Quirk, S. A. Boppart, and D. D. Sampson, Opt. Express 19, 6623 (2011).

[4] K. M. Kennedy, B. F. Kennedy, R. A. McLaughlin, and D. D. Sampson, Opt. Lett. 37, 2310 (2012).

[5] G. Gruca, S. de Man, M. Slaman, J. H. Rector, and D. Iannuzzi, Proc. SPIE 7503, 750381 (2009).

[6] D. Chavan, T. C. van de Watering, G. Gruca, J. H. Rector, K. Heeck, M. Slaman, and D. Iannuzzi, Rev. Sci. Instrum. 83, 115110 (2012).

[7] S. H. Yun, G. J. Tearney, J. F. de Boer, N. Iftimia, and B. E. Bouma, Opt. Express 11, 2953 (2003).

[8] J. Li, M. de Groot, F. Helderman, J. Mo, J. M. A. Daniels, K. Grünberg, T. G. Sutedja, and J. F. de Boer, Opt. Express 20, 24132 (2012).

[9] C. Joo, T. Akkin, B. Cense, B. H. Park, and J. F. de Boer, Opt. Lett. 30, 2131 (2005).

[10] D. Chavan, G. Gruca, T. van de Watering, K. Heeck, J. Rector, M. Slaman, D. Andres, B. Tiribilli, G. Margheri, and D. Iannuzzi, Proc. SPIE 8430 (2012).

Chapter -7

Commercial Prospects, Future Applications, and Conclusions

In this chapter, we present a ferrule-top nanoindenter setup designed for preclinical material property tests. The setup employs an extended version of the readout scheme that can provide a linear output also far from the quadrature point. This chapter also describes possible applications of ferrule-top cantilever probes for studying fundamental biological processes and in other areas of application.

7.1 NANOINDENTER FOR PRECLINICAL APPLICATIONS

7.1.1 Introduction

In previous chapters (Ch. 5 & 6) we demonstrated the use of ferrule-top cantilever probes for nanoindentation to assess the mechanical property of a PDMS sample in air and liquids. The readout used for those experiments allows one to tune the wavelength and use the linear part of the interference fringe to measure the deflection of the cantilever. This readout configuration, though sufficient for most experimental needs, limits the measurable linear deflection of the cantilever. As a result, the load applied during the indentation test is also limited. Furthermore, during the indentation of compliant samples, adhesive forces can cause the bending of the cantilever to go beyond the linear part of the interference fringe. In such cases, it is increasingly difficult to estimate the maximum adhesive force from the curve. To overcome these limitations, we demonstrate here an extended readout scheme which provides a linear cantilever displacement.

In this chapter, we also focus on the development of a nanoindentation instrument for preclinical studies. The system was designed to accommodate large sample sizes (up to few centimeters) and to allow large range X-Y automated sequential indentation. The instrument was also designed to perform in liquid environments to meet the prerequisite for most biomaterial indentation tests. We intend to promote the use of this instrument by clinicians and outside the research laboratories. Hence, efforts were made to make the instrument cost effective while maintaining the instrument specifications.

7.1.2 Extended Readout

The readout used in the previous ferrule-top nanoindentation experiments is based on Fabry-Pérot interferometry and uses a combination of a broad spectrum SLD source with a manual tunable filter. This readout allows one to tune the initial interference signal and adjust it to quadrature of the interference fringe. Thus the wavelength tunability of this readout maximizes the use of the linear part of the fringe. However, only the linear part of the interference fringe might not be sufficient for indentation tests that require larger depths and/or higher loads. The Fig. 7.1 shows the photodiode output when the cantilever is bent beyond the linear part of the interference fringe.

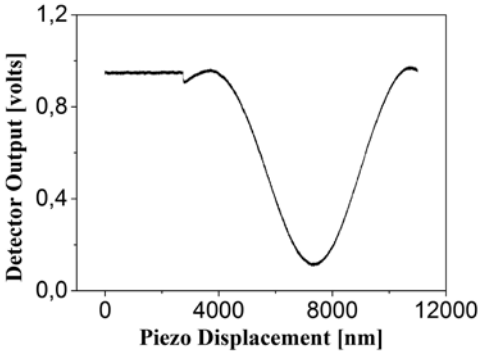

Fig. 7.1 Example of bending of a ferrule-top cantilever beyond the linear part of the interference fringe during the loading part of the indentation test.

The photodiode output (W) is a periodic function of the cavity gap (d) for a fixed wavelength of the laser (λ) and is given by the following equation:

$$W(d,\lambda) = W_0\left[1 + V\cos\left(\frac{4\pi d}{\lambda} + \varphi_0\right)\right] \tag{7.1}$$

where W_0 is the midpoint interference signal, V is the fringe visibility and φ_0 is a constant phase shift that depends on the geometry of the cantilever. It is necessary to transform this sinusoidal voltage output to a linear cantilever deflection (in nanometers) for further interpretation. In the literature, there are many methods suggested to overcome this challenge by generating two quadrature interference signals; either by the use of two optical fibers that are separated exactly by $\lambda/8$ [1] or by using two laser wavelengths [2]. Recently Karrai *et al* [3, 4] presented a technique of generating two quadrature signals by modulating the laser wavelength at high frequency (ω). In our new extended readout we employ a similar principle to generate two quadrature signals that combined, provide the bending of the cantilever. The schematic of the new readout is shown in Fig. 7.2.

The laser source consists of a broadband SLD source (Thorlabs) and a piezo-tunable optical filter (Lambda Quest, USA) [See APPENDIX A], which allows for wavelength selection and high frequency modulation of the wavelength. This wavelength modulation is achieved by applying a DC bias and a high frequency AC voltage via a function generator. The amplitude of the AC voltage was set to 20mV at 2 -3 kHz for most experiments.

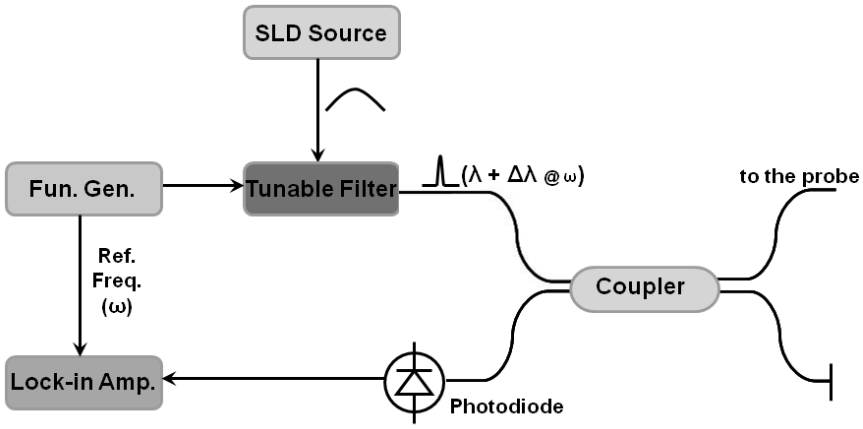

Fig. 7.2 Schematic of the extended readout.

The frequency of the wavelength modulation was chosen by taking into consideration the working bandwidth of the piezo-tunable filter and the rate of bending of the cantilever. This modulated wavelength light source ($\lambda_0 + \Delta\lambda \cos\omega t$) is then launched in the ferrule-top probe via a coupler as shown in the schematic. The photodiode output that gives the interference signal generated due to the bending of the cantilever is fed to a lock-in amplifier. The lock-in amplifier locks onto the first harmonic of the reference modulation frequency (ω) to generate a 90 degrees phase shifted signal. The details about the orthogonal signal processing to obtain a linear cantilever displacement are discussed in APPENDIX A. The linearized cantilever displacement calculated for the interference fringe in Fig. 7.1, is shown in Fig. 7.3.

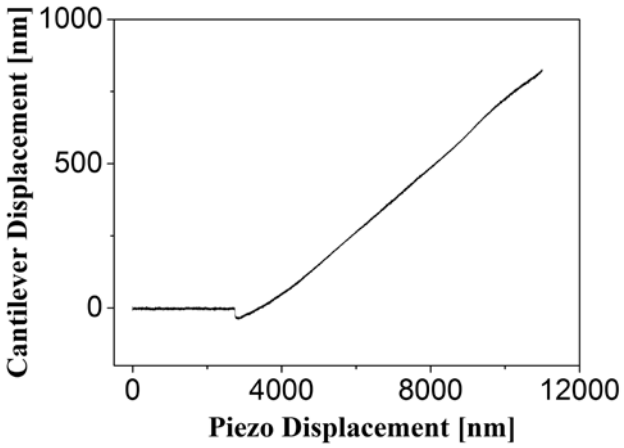

Fig. 7.3 Linearized cantilever displacement.

As shown in the figure above, the linearized cantilever displacement is now in a more usable form as compared to the sinusoidal curve of Fig. 7.1. It is important to note that the cantilever displacement shown here is the measured bending of the cantilever at the center (i.e. above the cleaved fiber end). Hence, one needs to take into account the right scaling factor to transform it to the cantilever tip displacement. The scaling factor can be estimated from the cantilever bending shape function based on its dimensions. Alternatively, it can also be estimated experimentally by bending the cantilever at its tip by a known amount of displacement stroke. As shown in Fig. 7.3, the linearized cantilever displacement still exhibits a low frequency sinusoidal component superimposed to the linear signal. An explanation to this effect can be found in Appendix A.

7.1.3 Nanoindenter Setup

The nanoindenter setup constructed for pre-clinical studies was built to accommodate large sample sizes, allow sequential XY indentation and be able to work in liquid testing environment. In the previously demonstrated indentation assembly (Fig. 5.3 Pg. 90), the sample was mounted on the Z piezoelectric translator which brings about the indentation stroke. A major disadvantage of this configuration is that it cannot support large samples without affecting the piezoelectric translator movement and dynamics. Also, the maximum piezoelectric translator stroke of ~100 μm limits large range sequential XY indentations for highly uneven sample surfaces.

In the new indentation setup shown in Fig. 7.4, the probe is mounted on the Z piezoelectric translator (PZS001 Thorlabs) that brings the indentation stroke. This translator is fitted with a surface mounted strain gauge that is connected to a strain gauge reader (TSG001 Thorlabs). The strain gauge reader provides the feedback to the piezoelectric translator voltage amplifier (TPZ001 Thorlabs) for closed-loop operations. The Z piezoelectric translator is further attached to a Z translation stage (PT1-Z8 Thorlabs) via an L - shape bracket. The Z translation stage, which has a travel range of 25 mm and step resolution of <50 nm, engages the probe with the sample described previously [5]. The extended range of the Z translation stage allows for sufficient retraction of the probe from the sample surface during the XY sequential indentation. The XY sequential indentation is realized by the XY translation stage (PT1-Z8 Thorlabs) as shown in the Fig. 7.4. The Z piezoelectric translator is covered with a polyurethane sheet to insulate it from liquid contact. The entire indenter setup is placed on a passive vibration isolation to reduce seismic noise. The data acquired during the indentation test are analyzed separately using an in-house developed data analysis program.

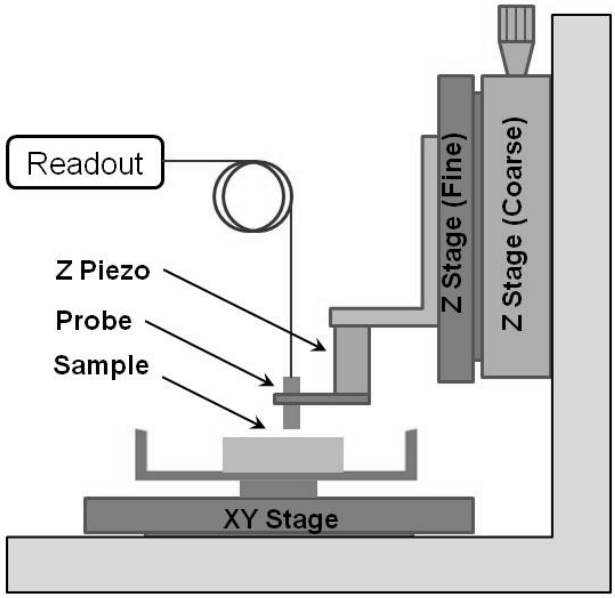

Fig. 7.4 Schematic view of new indentation setup (not to scale).

7.1.4 Results

In order to test the working principle of the new nanoindenter, we performed indentations on a swine ear cartilage, which was cut into 1 cm X 1 cm samples with flat surfaces. One of the samples was glued at the bottom of a petri dish filled with a buffer solution. The ferrule-top cantilever probe was lowered into the petri dish and allowed to establish thermal equilibrium.

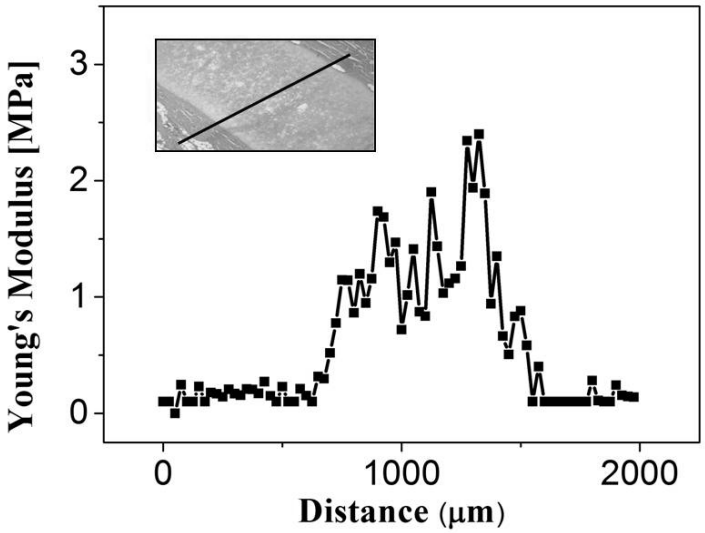

Fig. 7.5 Indentation line scan across swine ear cartilage sample.

After engaging the probe with the sample, a sequential indentation line scan in one dimension was performed over the sample. The sample was oriented such that the line scan covered three distinct areas (i.e. skin – cartilage – skin). The optical microscope image of the three distinct regions of the swine ear cartilage is shown in Fig. 7.5. Each indentation spot was 50 μm apart and was indented at the rate of ~0.5 μm/second. For each indentation spot, the indentation cycle consists of four phases: (i) probe-sample engagement; (ii) indentation stroke; (iii) probe retraction; and (iv) translation to next spot. The indentation data acquired for each spot was analyzed separately to calculate the Young's modulus for that spot. The calculated Young's modulus along the line scan is plotted in Fig. 7.5. The line scan exhibits higher Young's modulus for the cartilage region and lower modulus for the skin regions as expected.

The results clearly demonstrate the capability of the indenter setup and the ferrule-top probe for preclinical material property tests. The setup can contain large sample sizes and perform indentation in dry and wet testing environments. To promote the use of this technology, the indenter setup components were carefully chosen to keep the instrument cost as low as possible, while still meeting the performance criteria for a nanoindenter. The overall scheme was then taken over by a partnering company (Optics11 B.V.) that developed a commercial instrument for tissue engineering laboratories (see Fig. 7.6).

Fig. 7.6 Ferrule-top nanoindenter – PIUMA

7.2 FUTURE APPLICATIONS

7.2.1 Mechanotransduction & Chemiluminescence

Mechanotransduction and chemiluminescence are phenomena wherein a mechanical stimulus triggers a chemical reaction which in turn can be converted into a spectral response. This spectral response can be engineered depending on the nature of the chemical reaction involved. Active research is carried out on biological processes that exhibit these phenomena [6-8]. The study of these biological processes at cell and tissue level demands complex experimental techniques. Moreover, it is also important to investigate these phenomena as locally as possible. This puts a stringent demand on the experimental setup to have a compact ultra sensitive force transducer compatible with aqueous environment. Fiber-top and ferrule-top technologies, with their unique characteristics, can provide a solution for such experiments. Here we present two application areas where mechanotransduction and chemiluminescence can be used to understand some of the most fundamental biological processes.

7.2.1.1 Nitric Oxide Detection

Nitric Oxide (NO) is a widely known universal messenger and signaling molecule for various biological systems [9, 10]. Its abnormal production in the body is also linked to serious medical conditions like arteriosclerosis, cancer and rheumatoid arthritis [11], to name a few. Hence, there is a distinct scientific research area dedicated to fully understand the role of NO in various physiological processes.

One such area of research focuses on NO production and regulation due to external mechanical stimulus at tissue and cell levels. The primary challenges faced for NO detection are its high reactivity with surrounding biomolecules

and its extremely low concentration (nanomolar range). The high reactivity and low concentration of NO released makes it difficult for quantitative *in situ* measurements. Some of the mainstream techniques used for NO studies are chemiluminescence [12], electron paramagnetic resonance (EPR) spectroscopy [13], fluorescence [14] and electrochemical methods [15]. Each of these methods has its own merits and limitations and some of them are used in combination with mechanotransduction arrangements. Vatsa *et al* [6] demonstrated the regulation of NO production in a single bone cell by applying mechanical stimuli using an optical tweezers/micro needle. The NO production was measured using fluorescence microscopy technique. In another similar experiment, McGarry *et al* [7] proposed the use of AFM for the mechanical stimulus, hence making it possible to apply calibrated forces to bone cells. Although both these experimental techniques were demonstrated successfully, they still demand significant adaptation and development of the experimental setup. Furthermore, the NO production was measured optically using a microscope, thus limiting the achievable spatial resolution. To address these limitations, we propose an optic fiber force transducer with a NO selective functionalized indentation tip to detect *in situ* NO release.

The proposed device is based on a ferrule-top cantilever probe that combines scanning probe microscopy with spectroscopy [16]. The proposed capability of ferrule-top probe for mechanotransduction is well demonstrated in previous chapters. We propose NO selective functionalization of the optic fiber indentation tip to integrate NO detection capability in the probe. Studies in the past have demonstrated that heme proteins such as cytochrome c' exhibit spectral changes upon binding to NO [17, 18]. Kopelman *et al* [19] mobilized these heme proteins on the tip of an optical fiber to demonstrate NO sensitive optical fiber biosensor. We propose to implement a similar biochemical functionalization technique on the ferrule-top optic fiber indentation tip. The proposed experimental setup with optical detection scheme is shown in Fig. 7.7.

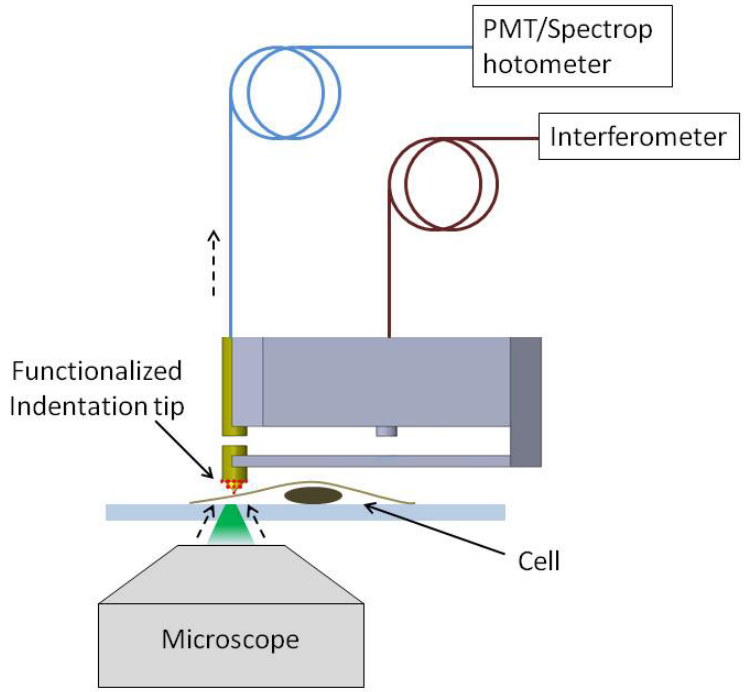

Fig. 7.7 Proposed ferrule-top probe and experimental setup for *in situ* NO detection

As shown in Fig. 7.7, the indentation tip is functionalized with NO sensitive biomolecules which exhibit a characteristic absorbance wavelength when illuminated with a broadband source. The absorbance peak shifts upon binding to NO and can be recorded via a spectrophotometer. Furthermore, by prior calibration of these sensors, the amount of NO released can also be quantified. The amount of mechanical force applied during the test is measured by the interferometer with nanonewton resolution. The proposed technique can be further optimized by using alternative mode of excitation and detection. Preliminary tests are under way to explore whether this scheme is viable or not.

7.2.1.2 Synaptic Vesicle Cycling

Living organisms are able to bring about coordinated functioning due to regulated signal transduction brought about by neurotransmitters. These neurotransmitters are actually vesicles containing signaling molecules that travel along the axon to a presynaptic terminal. These signaling molecules fuse with the membrane to release the content in synaptic space. The signaling molecules are detected by the receiver, which could be a neuron, or an effector cell of a tissue [20]. Studies have shown that after the release of their content, these vesicles are recycled for another round of neurotransmitter release and are organized into different pools [21, 22]. The cycling of these vesicles containing the signaling molecules has been a focus of active research to unravel the factors affecting signal transduction processes [23].

Burrone *et al.* presents a brief overview of various stimuli used to study the vesicle cycling process and presents the use of fluorescence probes to monitor vesicle cycling [8]. Apart from the stimuli enumerated in this article, efforts have also been made to study the effect of mechanical stimuli using atomic force microscope. Some of the major limitations for such studies are the complicated experimental requirement for localized stimuli. To address these issues, we envisage a ferrule-top cantilever probe in a similar configuration as shown in Fig. 7.7. For the proposed experiment, the target cells are fluorescently labeled as described previously [8] and the mechanical stimulus is provided by the ferrule-top tip. The photomultiplier tube can simultaneously record the intensity change in the fluorescently labeled cells. The observed intensity variation can provide insight into the mechanism of synaptic vesicle cycling.

The above mentioned experiments when designed carefully can unravel the understanding of these fundamental physiological processes. However some issues need to be addressed before these proposed techniques can be realized. The spring constant of the ferrule-top cantilever is still considerably high to perform nanoindentation of a single cell. Additionally, the optical signal

detection scheme needs to be optimized to achieve required sensitivity. Also for this application, our group has initiated a first series of tests that aim at addressing the issues illustrated above.

7.2.2 Other Applications

In the previous section, we proposed two areas of application for ferrule-top cantilever probe that exploits its nanonewton force sensitivity and optical detection capability. In the commercial context, we envisage an interesting application area with OLED (organic light emitting diode) indentation, where the capabilities of a ferrule-top probe can be utilized. OLEDs are fabricated by sandwiching an organic electroluminescent layer between the metal electrodes. Though OLED technology has become of commercial interest, some fundamental questions related to its competitive advantages still remain unanswered. It is for example well known that, during the fabrication of OLED displays, humidity is an undesirable factor which can deteriorate the organic layer and give rise to pin-holes (black pixels) [24]. In spite of this widely known challenge, very limited progress has been made in understanding the formation and growth of these pin-holes. In the past, efforts were made to image the electroluminescent organic layer by using a conducting AFM tip [25]. However such experiments do not provide insight into the optical properties of the organic layer. Ferrule-top cantilever probe with careful fabrication can perform conductive AFM imaging and simultaneously probe the optical properties of the electroluminescent layer. This idea has been now under discussion with a few industrial partners, who may be interested to use ferrule-top technology to better understand the relation between pixel failure rate and fabrication conditions.

7.3 CONCLUSIONS

In this chapter we presented an extended readout for ferrule-top probes, demonstrated and proposed new experimental setups and envisaged few fundamental as well as commercial areas of application. Each of the application area mentioned in this chapter (*Nitric Oxide Detection*, *Synaptic Vesicle Cycling* and *OLED Indentation*) requires significant research and development on various experimental aspects of probe fabrication, setup design, chemical sensing and optical signal optimization. Still, each of those applications represents a tantalizing opportunity to extend the range of fields in which ferrule-top technology may, on day, make the difference.

REFERENCES

[1] K. A. Murphy, M. F. Gunther, A. M. Vengsarkar, and R. O. Claus, Opt. Lett. 16, 273 (1991).

[2] O. B. Wright, Op. Lett. 16, 56 (1991).

[3] K. Karrai, Patent WO2009043421 (A1) (2009).

[4] K. Karrai and P. F. Braun, Proceedings EUSPEN 2010 156V1 (2010).

[5] D. Chavan, T. C. van de Watering, G. Gruca, J. H. Rector, K. Heeck, M. Slaman, and D. Iannuzzi, Rev. Sci. Instrum. 83, 115110 (2012).

[6] A. Vatsa, D. Mizuno, T. H. Smit, C. F. Schmidt, F. C. MacKintosh, and J. Klein-Nulend, J. Bone Miner. Res., 21, 1722 (2006).

[7] G. McGarry, P. Maguire, V. A. Campbell, B. C. O'Connell, P. J. Prendergast, S. P. Jarvis, J. Orthop. Res., 26, 513 (2008).

[8] J. Burrone, Z. Li, and V. N. Murthy, Nat. Protocals. 1, 2970 (2006).

[9] L. J. Ignarro, Nitric Oxide Biology and Pathobiology, Academic Press (Book).

[10] T. Nagano, and T. Yoshimura, Chem. Rev. 102, 1235 (2002).

[11] X. Ye, S. S. Rubakhin, and J. V. Sweedler, Analyst. 133, 423 (2008).

[12] A. M. Leone, V. W. Furst, N. A. Foxwell, S. Cellek, and S. Moncada, Biochem. Biophys. Res. Commun., 221, 37 (1996).

[13] T. Yoshimura, H. Yokoyama, S. Fujii, F. Takayama, K. Oikawa, and H. Kamada, Nat. Biotechnol., 14, 992 (1996).

[14] H. Kojima, N. Nakatsubo, K. Kikuchi, S. Kawahara, Y. Kirino, H. Nagoshi, Y. Hirata, and Tetsuo Nagano, Anal. Chem., 70, 2446 (1998).

[15] K. Shibuki, Neurosci. Resear., 9, 69 (1990).

[16] D. Chavan, G. Gruca, T. van de Watering, K. Heeck, J. Rector, M. Slaman, D. Andres, B. Tiribilli, G. Margheri, and D. Iannuzzi, Proc. SPIE 8430 (2012).

[17] S. L. R. Barker, T. E. Meyer, M. A. Cusanovich, and R. Kopelman, Anal. Chem., 70, 4902 (1998).

[18] L. G. Quaroni, H. E. Seward, K. J. McLean, H. M. Girvan, T. W. B. Ost, M. A. Noble, S. M. Kelly, N. C. Price, M. R. Cheesman, W. E. Smith, and A. W. Munro, Biochemistry, 43, 16416 (2004).

[19] S. L. R. Barker, Y. Zhao, M. A. Marletta, and R. Kopelman, Anal. Chem., 71, 2071 (1999).
[20] R. Stufflebeam, Proc. Consort. Cognit. Sci. Instruct, 374 (2008).

[21] T. Schikorski, and C. F. Stevens, Nat. Neurosci. 4, 391 (2001).

[22] S.O. Rizzoli, and W. J. Betz, Science 303, 2037(2004).

[23] T. C. Suedhof, Annu. Rev. Neurosci. 27, 509 (2004).

[24] L. Ke, S. F. Lim, and S. J. Chua, J. of Poly. Sci. B, 39, 1697 (2001).

[25] H. Lin, S. Chen, Y. Lee, and S. Chen, J. Vac. Sci. Technol. B, 19, 308 (2001).

Appendix A

Extended Readout

A piezo-tunable optical filter (Lambda quest, USA) is connected to a broadband SLD source and a DC bias voltage is applied in discrete steps. The wavelength output by the optical filter with respect to the DC voltage applied is shown in Fig. A.1.

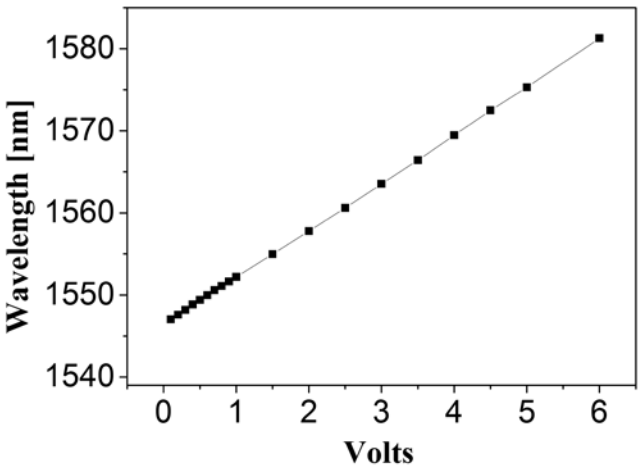

Fig. A.1. Wavelength output at the exit of the piezo-tunable optical filter as a function of voltage applied.

During the experiments, a DC voltage is applied to the piezo-tunable optical filter to tune the output to the center wavelength of the SLD λ_0 (~1550 nm). A high frequency, ~20 mV AC voltage , added to the DC bias, allows one to superimpose a wavelength modulation $\Delta\lambda$ (~0.1 nm). Hence the wavelength output from the piezo-tunable optical filter can be represented by the following equation:

$$\lambda = \lambda_0 + \Delta\lambda \cos wt \tag{A.1}$$

where w is the modulation frequency.
As already explained earlier in the thesis, the photodiode output of the readout (W) is a periodic function of the cavity gap (d) for a fixed wavelength of the laser (λ) and is given by the following equation:

$$W(d,\lambda) = W_0\left[1 + V\cos\left(\frac{4\pi d}{\lambda} + \varphi_0\right)\right] \tag{A.2}$$

where W_0 is the midpoint interference signal, V is the fringe visibility and φ_0 is a constant phase shift that depends on the geometry of the cantilever. With the implementation of the wavelength modulation scheme, the photodiode output can be represented by the following equation:

$$W(d,\lambda) = W_{DC} + W_\omega \cos wt \tag{A.3}$$

where

$$W_{DC} = W_0(1 - V\cos(4\pi d/\lambda_0) \tag{A.4}$$

and

$$W_{\omega} = \frac{4\pi\Delta\lambda V W_0}{\lambda_0^{\,2}} \sin(4\pi d / \lambda_0) \qquad \text{(A.5)}$$

The linearization procedure stems from the fact that, in this configuration, W_{DC} and $W\omega$ can be separately monitored. W_{DC} can in fact be obtained as the output of the photodiode of the readout after low pass frequency filtering, whereas $W\omega$ can be measured via a lock-in amplifier locked to the modulation frequency w. Importantly, these two signals are phase-shifted by 90^0, as illustrate in Fig. A.2, where, for the sake of clarity, we reported only the loading part of one indentation curve obtained while indenting a hard surface (a glass sample).

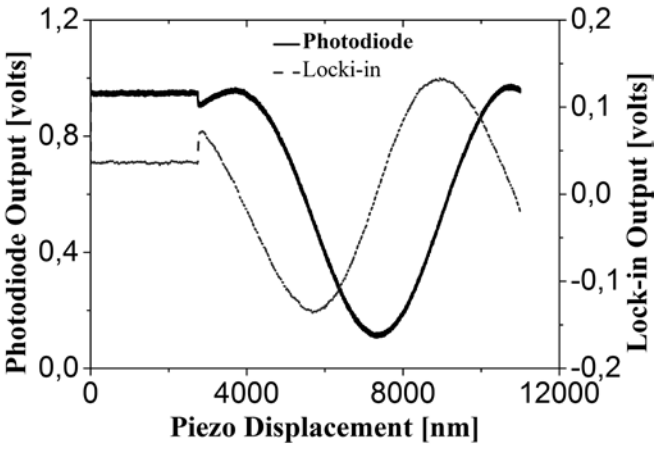

Fig. A.2 Two orthogonal signals obtained from the photodiode and the lock-in.

These two orthogonal signals after appropriate scaling can be plotted in a Lissajous curve, as shown in Fig. A.3.

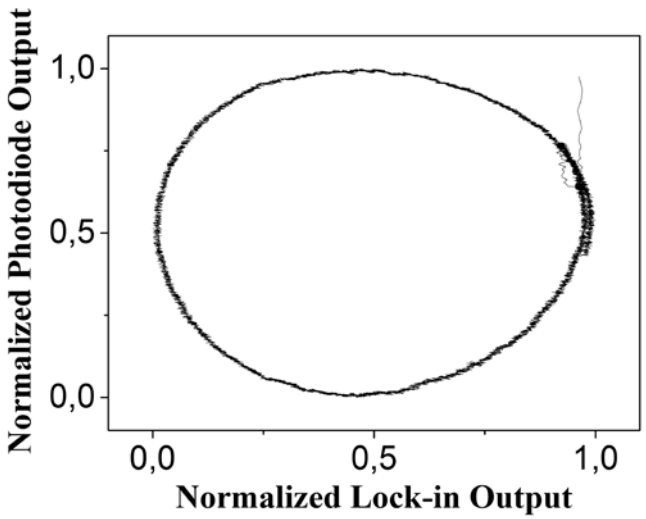

Fig. A.3. Lissajous curve for two orthogonal signals.

The {X,Y} data points of this unit circle correspond to consecutive deflections of the cantilever *d*, given by the following equation:

$$d = \frac{\lambda_0}{4\pi}\arctan(Y, X) \tag{A.6}$$

Unwrapping the phase of *arctan(Y/X)* allows one to calculate *d* from multiple interference fringes. Of course, the *arctan* function, being a periodic function, has a discontinuity every $\lambda_0/2$. This can be solved by concatenating each sequential $\lambda_0/2$ unwrapped phase to obtain the linear cantilever deflection as shown in Fig. A.4 (same as Fig. 7.4).

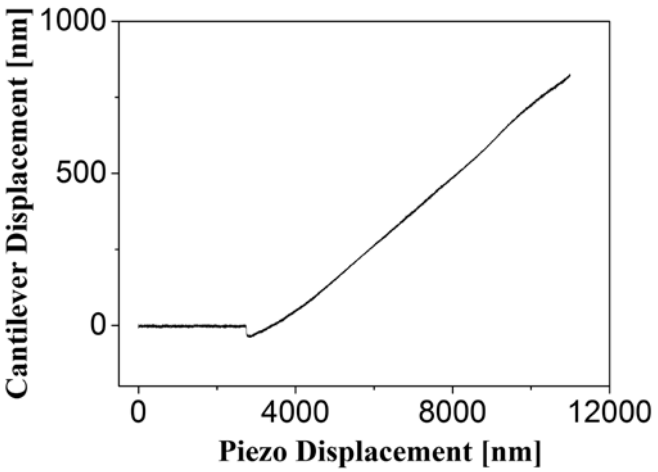

Fig. A.4. Linearized cantilever displacement.

The linearized cantilever displacement shown in the figure above exhibits a low frequency sinusoidal component superimposed on the cantilever displacement. Our understanding suggests that this effect is due to the fact that the gap between the cleaved fiber and the cantilever is not a single cavity. This problem originates from the design and fabrication process adopted for the ferrule-top cantilever probe. During the fabrication of the ferrule-top probe, a portion of the cantilever above the cleaved fiber has a hole which is filled by transparent UV curable glue. This results into two reflecting surfaces, the bottom surface and the top surface of the filled hole. This problem is now addressed by filling the hole with a non-transparent epoxy.

Summary

Currently, scanning probe microscopy and nanoindentation are two widely used techniques for the characterization of materials at nanoscale. These techniques are used to investigate physical, chemical, thermal, electrical and optical properties of a material. Although these techniques have contributed significantly to material research, their use outside the research laboratory is restricted due to the complexity of the instrument. Hence, novel developments that bring about step change in instrumentation and functionality of these techniques can help to expand their application areas.

The work presented in this thesis focuses on the development of a new technology platform – *fiber-top* technology, as a tool for material property characterization at nanoscale. The research done towards the development of this technology was highly multidisciplinary and encompasses areas of optic fiber sensing, micro-technology/micro-fabrication, control systems, optics and biomaterials. The thesis work can broadly be divided into two important application areas of *fiber-top* technology: (i) Scanning probe microscopy and (ii) Nanoindentation.

The concept of *fiber-top* technology – carving a cantilever on top (cleaved end) of an optical fiber was introduced by D. Iannuzzi *et al* in 2006. In such a *fiber-top* device, a laser when shone from the other end of the optical fiber, travels along the optic fiber core and emerges at the face of the optical fiber. Part of this light reflects back and a part transmits further to be reflected by the surfaces of the cantilever. These reflected signals travel back though the same optical fiber and are redirected on a photodiode. With this detection scheme, the deflection of the *fiber-top* cantilever can be measured with sub-nanometer resolution.

In the first chapter of this thesis, the background and the principle of scanning probe microscopy are discussed, followed by an introduction to the

concept of *fiber-top* technology, its detection scheme, working principle and limitations. The next chapter introduces a novel cost effective fabrication process as an alternative to *fiber-top* technology. In this new concept called *ferrule-top* technology, a cantilever is fabricated on top of a ferruled optical fiber. The chapter also discusses the fabrication of a ferrule-top atomic force microscope (AFM) probe and the construction of a fully functional AFM setup. This AFM setup successfully demonstrates contact mode imaging of a sample in air and liquid environment.

The third chapter incorporates improvements in the ferrule-top probe fabrication process and further extends its capabilities as a versatile tool for nanoscale imaging. Here, in the first part of the chapter we demonstrate tapping mode and contact mode imaging performed at 12 degree Kelvin. In the second part, we integrate the ferrule-top probe into a high speed AFM scanner and perform contact mode imaging up to 2 frames/second. The fourth chapter focuses on an important and unique capability of *fiber-top* technology of combining scanning probe microscopy with near field optical microscopy (SNOM), i.e. able to simultaneously investigate topography and optical property of a sample. Here we demonstrate two different approaches adopted for the fabrication of a *fiber-top* and a ferrule-top probe with near field capabilities. The results obtained demonstrate that the *fiber-top* and the ferrule-top technology can provide multiple advantages over the conventional SNOM techniques.

The work presented in the fifth chapter focuses on the development of ferrule-top technology for application area of Nanoindentation. Ferrule-top technology provides unique advantages over conventional indentation instruments in terms of better force resolution, easy of handling and ability to perform indentation testing in liquid environment. The results obtained from indentation testing of various polymers demonstrate the full functionality of a ferrule-top indentation probe. In the following chapter, we extend the capability of ferrule-top probe to perform optical coherence elastography (OCE) by combining indentation and optical coherence tomography (OCT) in a specially fabricated ferrule-top probe called OMNE (OptoMechanical NanoElastography) probe. This probe allows one to

impart calibrated load with nanonewton force resolution to a sample and simultaneously observe the material deformation within the sample during the indentation stroke.

The final chapter presents some of the latest developments of ferrule-top nanoindenter to accommodate large sample sizes and scan areas, as a step towards preclinical indentation trials. Furthermore, this chapter also discusses other areas of applications wherein ferrule-top technology can be used to study fundamental biological processes by means of mechanotransduction and chemiluminescence. Finally, *fiber-top* technology that was invented serendipitously has matured tremendously over the years and is being commercialized by a spin-off company (Optics11 BV).

Samenvatting

Tegenwoordig zijn scanning probe microscopie en nanoindentatie twee vaak gebruikte technieken voor het karakteriseren van materialen met nanometer resolutie. Deze technieken worden gebruikt voor het onderzoeken van fysieke, chemische, thermische, elektrische en optische eigenschappen van een materiaal. Hoewel deze technieken een significante bijdrage hebben geleverd aan het onderzoek van materiaal, wordt het nog weinig gebruikt buiten het laboratorium vanwege de complexiteit van de instrumentaten. Daarom zijn nieuwe ontwikkelingen die de instrumenten versimpelen en de toepasbaarheid vergroten van groot belang.

Dit proefschrift focust zich op de ontwikkeling van een nieuw technologisch platform – *fiber-top* technologie - als een hulpmiddel voor het bepalen van materiaaleigenschappen op nanometerschaal. Het onderzoek dat nodig was bij het ontwikkelen van deze techniek was zeer multidisciplinair en omvatte toepassingsgebieden als 'fiber sensing', micro-technologie/micro-fabricatie, feedback systemen, optica en biomaterialen. Dit proefschrift kan ruwweg worden onderverdeeld in twee belangrijke toepassingsgebieden van *fiber-top* technologie: (i) Scanning probe microscopie en (ii) Nanoindentatie.

Het concept van *fiber-top* technologie – het uitsnijden van een cantilever op het uiteinde (afgesneden eind) van een optische vezel – werd geïntroduceerd door D. Iannuzzi *et al.* in 2006. In zo'n *fiber-top* instrument wordt een laser door de kern van een optische vezel geschenen. Een deel van het licht wordt gereflecteerd door het uiteinde van de optische vezel, de rest reist verder en wordt gereflecteerd door de cantilever. Het gereflecteerde licht reist samen terug door dezelfde optische vezel en wordt gedetecteerd door een detector. Met dit detectieschema kan de beweging van een *fiber-top* cantilever worden gemeten met subnanometer resolutie.

In het eerste hoofdstuk van dit proefschrift wordt de achtergrond en het principe van scanning probe microscopie beschreven, gevolgd door: een introductie van het concept *fiber-top* technologie, het detectie schema, het principe en de beperkingen. Het volgende hoofdstuk beschrijft een nieuwe kostenbesparende fabricatie methode als een alternatief voor *fiber-top* technologie. Bij dit nieuwe concept, ferrule-top technologie genaamd, wordt een cantilever uitgesneden op het uiteinde van een in een ferrule gestoken optische vezel. Ook wordt de fabricatie van een atomic force microscoop (AFM) probe en de constructie van een volledig functioneel AFM systeem besproken. Dit AFM systeem demonstreert 'contact mode imaging' van een monster in lucht en in vloeistof.

Het derde hoofdstuk bevat verbeteringen in het ferrule-top probe fabricatie proces, dit vergroot de mogelijkheden van dit veelzijdige hulpmiddel voor beeldvorming op de nanometer schaal. In het eerste deel van het hoofdstuk demonstreren we 'tapping mode' en 'contact mode imaging' bij een temperatuur van 12 Kelvin. In het tweede deel van het hoofdstuk integreren we een ferrule-top probe in een hogesnelheids AFM en doen we contact mode imaging met een snelheid tot twee frames per seconde. Het vierde hoofdstuk focust op een belangrijke en unieke toepassing van *fiber-top* technologie; het combineren van scanning probe microscopie met near field optische microscopie (SNOM), wat het gelijktijdig verkrijgen van informatie over de topografie van het monsteroppervlak en zijn optische eigenschappen mogelijk maakt. De verkregen resultaten laten zien dat *fiber-top* en ferrule-top technologie meerdere voordelen kunnen hebben ten opzichte van conventionele SNOM technieken.

Het werk in het vijfde hoofdstuk focust op de ontwikkeling van ferrule-top technologie voor het toepassingsgebied van de nanoindentatie. Ferrule-top technologie heeft unieke voordelen ten opzichte van conventionele indentatie technieken in de zin van een betere krachresolutie, het gebruiksgemak en de mogelijkheid om nanoindentatie experimenten uit te voeren in vloeistof. De resultaten van indentatie testen op verschillende polymeren laten de volledige functionaliteit van ferrule-top probes zien. In het volgende hoofdstuk vergroten we de mogelijkheden van ferrule-top

probes door het uitvoeren van 'optical coherence elastography' (OCE) door het combineren van indentatie en 'optical coherence tomography' (OCT) met een speciaal ontwikkelde ferrule-top probe, OMNE (OptoMechanical NanoElastography) probe genaamd. Deze probe maakt het mogelijk om, met nanonewton resolutie, kracht uit te oefenen op het monster en tegelijkertijd de vervorming waar te nemen.

Het laatste hoofdstuk presenteert een aantal van de laatste ontwikkelingen op het gebied van de ferrule-top nanoindenter voor het scannen van grote oppervlaktes, als een stap in de richting van preklinische testen. Verder bespreekt dit hoofdstuk ook andere toepassingsgebieden waarbij ferrule-top technologie een rol kan spelen, zoals het bestuderen van biologische processen door middel van mechanotransductie en chemieluminescentie. Over de jaren *fiber-top* technologie is enorm gegroeid en inmiddels nu gecommercialiseerd door een spin-off bedrijf (Optics 11 BV).

List of Publications

1. **Chavan, D.**, Gruca, G., de Man, S., Slaman, M., Rector, J.H., Heeck, K., Iannuzzi, D., 2010. Ferrule-top atomic force microscope. Review of Scientific Instruments 81, 123702.

2. **Chavan, D.**, Andres, D., Iannuzzi, D., 2011. Ferrule-top atomic force microscope. II. Imaging in tapping mode and at low temperature. Review of Scientific Instruments 82, 046107.

3. Gavan, K.B., Rector, J.H., Heeck, K., **Chavan, D.**, Gruca, G., Oosterkamp, T.H., Iannuzzi, D., 2011. Top-down approach to fiber-top cantilevers. Optics Letters 36, 2898-2900.

4. Tiribilli, B., Margheri, G., Baschieri, P., Menozzi, C., **Chavan, D.**, Iannuzzi, D., 2011. Fibre-top atomic force microscope probe with optical near-field detection capabilities. Journal of Microscopy 242, 10-14.

5. **Chavan, D.**, Gruca, G., van de Watering, T., Heeck, K., Rector, J., Slaman, M., Andres, D., Tiribilli, B., Margheri, G., Iannuzzi, D., 2012. Fiber-top and ferrule-top cantilevers for atomic force microscopy and scanning near field optical microscopy. ProcSPIE, vol. 8430, p. 84300Z.

6. **Chavan, D.**, van de Watering, T.C., Gruca, G., Rector, J.H., Heeck, K., Slaman, M., Iannuzzi, D., 2012. Ferrule-top nanoindenter: An optomechanical fiber sensor for nanoindentation. Review of Scientific Instruments 83, 115110.

7. Gruca, G., **Chavan, D**., Cipullo, A., Babaei Gavan, K., De Filippis, F., Minardo, A., Rector, J., Heek, K., Zeni, L., Iannuzzi, D., 2012. Development of fiber optic ferrule-top cantilevers for sensing and beam-steering applications. Proc SPIE, vol. 8439, p. 84390E.

8. Chang, P.I., **Chavan, D**., Paris, R., Iannuzzi, D., Schitter, G., 2013. Towards High Speed Ferrule-Top Atomic Force Microscopy. Proceedings of the 6th IFAC Symposium on Mechatronic Systems 51, 131-137.

9. **Chavan, D**., Mo, J.H., de Groot, M., Meijering, A., de Boer, J.F., Iannuzzi, D., 2013. Collecting optical coherence elastography depth profiles with a micromachined cantilever probe. Optics Letters 38, 1476-1478.

10. Gruca, G., **Chavan, D**., Rector, J., Heeck, K., Iannuzzi, D., 2013. Demonstration of an optically actuated ferrule-top device for pressure and humidity sensing. Sensors and Actuators a-Physical 190, 77-83.

Acknowledgement

I would like to express my gratitude to all those who were part of my PhD journey during the last four years.

Curriculum Vitae

Dhwajal Chavan was born in Baroda (Vadodara), India in 1982. He received his Bachelors degree in Mechanical Engineering from India and Masters in Mechatronics from Aachen University of Applied Sciences, Germany. He performed his master thesis at University of Twente, The Netherlands in the field of nanoscale deposition using atomic force microscope. He continued to work at University of Twente as a researcher for a period of 14 months on the topic of fabrication and characterization of MEMS transducers. In April 2009, he joined the group of Prof. Dr. Davide Iannuzzi at Vrije Universiteit, Amsterdam to perform his doctorate work on the topic of *fiber-top* technology for material science research. In April 2013, he joined Shell Global Solutions International BV, Rijswijk, The Netherlands as Research Geophysicist.